Benemérita Universidad Autónoma de Puebla

Facultad de Ciencias Físico Matemáticas

Properties of a Higgs boson at 95 GeV at LHC

T E S I S

QUE PARA OPTAR POR EL GRADO DE:

Licenciatura en Física

PRESENTA:

Oswaldo Alan Vergara Eslava

DIRECTOR:

Alan Ignacio Hernández Juárez y Arturo Fernández Téllez

(Puebla, pue), octubre, 2025

Título: Properties of a Higgs boson at 95 GeV at LHC
Estudiante: Oswaldo Alan Vergara Eslava

COMITÉ

Gilberto Tavares Velasco
Presidente

Héctor Novales Sánchez
Secretario

Jesús Ricardo Alvarado García
Vocal

Suplente

Alan Ignacio Hernández Juárez y Arturo Fernández Téllez
Asesor

Agradecimientos

La presente tesis se fundamenta en la inspiración proporcionada por las contribuciones de mis asesores, el Dr. Alan Ignacio Hernández Juárez y el Dr. Arturo Fernández Téllez, quienes dedicaron tiempo, apoyo y paciencia a mi desarrollo académico. Su orientación y correcciones fueron fundamentales, motivándome a superar mis expectativas en la elaboración de este trabajo.

Esta dedicatoria se extiende a todas las personas que, directa o indirectamente, contribuyeron a mi proceso de estudio y aprendizaje, especialmente a mis padres, quienes me brindaron la libertad necesaria para madurar y progresar en cada etapa académica; a mis tíos y abuelos, por su hospitalidad; y a mis amigos y pareja, por su compañía y soporte en momentos desafiantes. En esta tesis, se refleja el impacto de todos ellos.

Declaración de autenticidad

Por la presente declaro que, salvo cuando se haga referencia específica al trabajo de otras personas, el contenido de esta tesis es original y no se ha presentado total o parcialmente para su consideración para cualquier otro título o grado en esta o cualquier otra Universidad. Esta tesis es resultado de mi propio trabajo y no incluye nada que sea el resultado de algún trabajo realizado en colaboración, salvo que se indique específicamente en el texto.

Oswaldo Alan Vergara Eslava. (Puebla, pue), octubre, 2025

Resume

After the discovery of the 125 GeV Higgs boson, several small but persistent excesses near 95 GeV in $\gamma\gamma$, $\tau^+\tau^-$ and $\bar{b}b$ final states reported by CMS, ATLAS and LEP have revived the search for an additional scalar. Motivated by these anomalies, we study a hypothetical Higgs-like state ϕ at $m_\phi = 95.4$ GeV produced via gluon fusion at the LHC. Using an effective Lagrangian, analytic decay-width formulae are obtained for $\phi \to \gamma\gamma$, $\tau^+\tau^-$ and $\bar{b}b$, introducing CP-even/odd form factors h_1, h_3 and scalar/pseudoscalar couplings g_s, g_p. Three production benchmarks ($\kappa = 1, \frac{1}{2}, 2$) simulate potential variations in the gluon–fusion cross-section. A parameter scan, constrained by the measured signal strengths $\mu_{\gamma\gamma}$, $\mu_{\tau\tau}$, and μ_{bb}, delineates closed annular regions of allowable values for h_1, h_2 in the $\phi \to \gamma\gamma$ decay, and g_s, g_p in the $\phi \to \tau^+\tau^-$, $\bar{b}b$ decays.

Contents

List of Figures

List of Tables

Chapter 1

Higgs Physics in the Standard Model.

The Standard Model (SM) represents the most widely accepted theoretical framework for describing three of the four fundamental forces of nature: electromagnetic, weak, and strong interactions. Gravity remains outside this framework, being described separately by General Relativity. The theory posits that these fundamental interactions are mediated by force-carrying particles known as bosons.

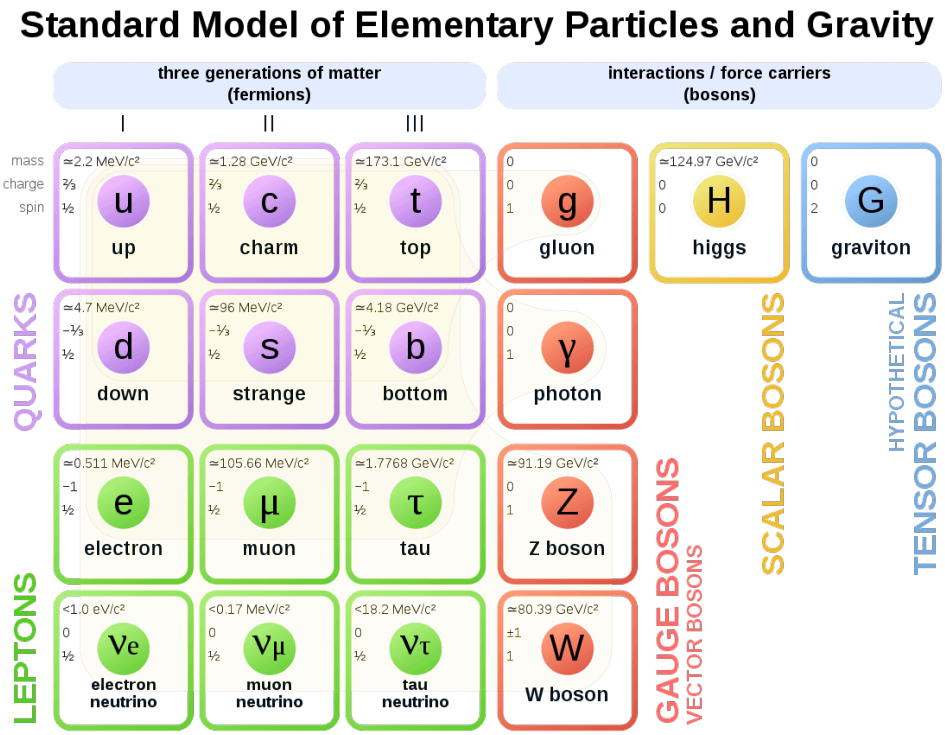

Figure 1.1: Standard model of elementary particles

Within this framework, matter is primarily composed of fermions, which include leptons and quarks, while bosons serve as mediators of the fundamental interactions (Figure 1.1). There are six leptons in the SM, consisting of the electron (e), muon (μ), tau (τ), and their respective neutrinos (ν_e, ν_μ, and ν_τ). Quarks are similarly classified into six distinct flavors: up (u), down (d), charm (c), strange (s), top (t), and bottom (b). With respect to the bosons, the photon (γ) serves as the mediator of electromagnetic interactions, influencing charged particles; the W and Z bosons facilitate weak interactions, which are instrumental in processes such as beta decay; and the gluons (g) are responsible for mediating the strong force that binds quarks together

within protons and neutrons, amongst other composite particles. The graviton, a hypothetical particle proposed as the quantum mediator of gravity, remains unobserved experimentally, being one of the key limitations of the Standard Model. Finally, the Higgs boson (H) is fundamental to the Higgs mechanism, which imparts mass to both fermions and gauge bosons through spontaneous symmetry breaking [17].

The SM scalar sector provides a framework in which the electroweak symmetry is spontaneously broken via the Higgs mechanism. This mechanism introduces a scalar field whose quantum excitation corresponds to the Higgs boson. The coupling of the Higgs field to gauge bosons and fermions allows particles to acquire mass in a gauge-invariant manner. The SM predicts a single neutral scalar boson, with couplings that are proportional to the masses of the particles it interacts with. At tree level, the Higgs boson does not couple to photons or gluons, but effective couplings arise through quantum loops involving charged or colored particles [21].

1.1 Electroweak Symmetry and spontaneous symmetry break

The electroweak theory unifies electromagnetic and weak interactions under the gauge symmetry $SU(2)_L \times U(1)_Y$ at high energies. This symmetry governs weak interactions. Only left-handed fermions feel this force: they are organized in doublets under $SU(2)_L$ with weak third isospin component $T_3 = \pm t\frac{1}{2}$, while right-handed fermions are singlets ($T_3 = 0$). Each field also carries a weak hypercharge Y associated with $U(1)_Y$, chosen so that when the symmetry breaks it reproduces the electrical charge $Q = T_3 + \frac{Y}{2}$. For example, the left-handed electron e_L forms a doublet with its neutrino $(\nu_e, e)_L$ of $Y = -1$, while e_R is a singlet with $Y = -2$; so you get $Q = -1$ for the electron and $Q = 0$ for ν_e.[21]

In the unified scheme of the symmetry $SU(2)_L \times U(1)_Y$, equations require that force-bearing bosons ($W^{\pm}$ and Z) are initially massless to respect the mathematical symmetry of the theory. However, in the wild, we observe that the W and Z bosons do have mass (80 GeV and 91 GeV respectively),while the photon (electromagnetic carrier) remains massless. This discrepancy indicates that electroweak symmetry must be broken in some way: at low energies, the weak interaction appears differentiated (short-range by heavy bosons) while the electromagnetic one remains long-range with photons without mass [10][11].

The solution proposed in 1964 by François Englert, Robert Brout, and Peter Higgs, among others, was to introduce the idea of a spontaneous rupture of symmetry in the gauge context. In a spontaneous breakdown of symmetry, the laws of the system respect symmetry, but the physical state of the system does not. The Higgs field (a complex scalar doublet with two neutral and two charged components) acquires an expected value in the vacuum $v \approx 246$ GeV in a particular direction of the field space. This produces a spontaneous breakout of $SU(2)_L \times U(1)_Y$ towards the residual symmetry $U(1)_{\text{em}}$ of electromagnetism [25]. Graphically, spontaneous rupture of electroweak symmetry is often illustrated with a potential in the form of a 'Mexican hat' for the Higgs field. In this potential (Figure 1.2), the state of minimum energy is not in the symmetrical center, but in a degenerate 'crown' of equivalent states. The field spontaneously chooses one of those vacuum states (a point in the crown), breaking the symmetry but not modifying the underlying laws. A common analogy is a perfectly balanced pencil on its tip: the initial situation is symmetrical (any direction is equivalent) but unstable, and at the slightest fluctuation, the pencil will fall in some direction randomly, breaking the symmetry even though the underlying laws remain symmetrical [22].

Mathematically, when a continuous symmetry breaks, modes of zero energy excitation called Goldstone bosons arise. In this case, the Higgs doublet has 4 degrees of real freedom; after

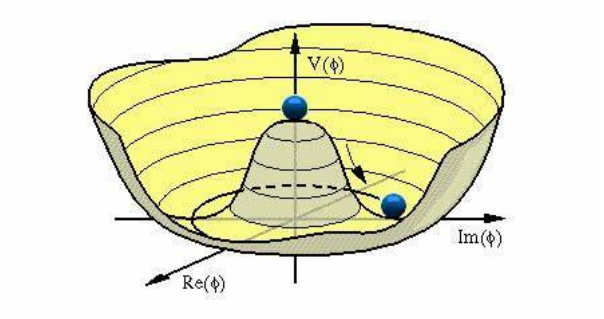

Figure 1.2: Representation of the potential of Higgs ("Mexican Hat"). The Higgs field (ϕ) has a non-zero vacuum value (minimum of energy outside the origin), which breaks the original symmetry and generates masses for W and Z while the photon remains massless [29]

.

the breakup, 3 of them would behave like massless Goldstone bosons. However, due to gauge invariance, these degrees of freedom do not appear as physical particles: they are absorbed by the gauge bosons $W^{\pm}$ and Z^0, giving them the additional longitudinal components that lead to mass. This is the core of the Higgs mechanism: the W and Z bosons "eat" the Goldstones and become massive, while the only degree of remaining freedom of the Higgs field manifests the observable scalar particle: the Higgs boson. In short, the $SU(2)_L \times U(1)_Y$ symmetry breaks spontaneously and the vacuum chooses a particular direction in the Higgs space; this allows mass to be given to particles without explicitly breaking the fundamental gauge symmetry. [15].

1.2 Higgs mechanism: mass generation for gauge bosons and fermions.

The Higgs mechanism formalizes the above; it proposes that there is an omnipresent scalar field (H) with a vacuum expected value different from zero [21]. The elemental particles that interact with this field acquire mass, while non-interacting particles remain massless. In particular, the $W^{\pm}$ and Z^0 bosons get high masses by coupling strongly with the Higgs field, while the photon does not couple at all and so it remains massless. Thus, the Higgs 'breaks' electroweak symmetry by providing mass to the gauge bosons of weak interaction and making this force short-range (since massive particles cannot propagate long-distance interactions) [11]. In detail, electroweak gauge bosons acquire mass when interacting with Higgs condensate. As the Higgs field expands around its vacuum value $v \approx 246$ GeV, mass terms appear for $W^{\pm}$ and Z^0. The resulting formulas at tree level are:

- $W^{\pm}$ mass: $m_W = \frac{1}{2}gv$, where g is the $SU(2)_L$ constant. Using $g \approx 0.65$, $m_W \approx 80$ GeV is predicted, in good agreement with the experimental value (80.4 GeV).
- Z^0 mass: $m_Z = \frac{v}{2}\sqrt{g^2 + g'^2}$, where g' is the $U(1)_Y$ constant. Equivalently, $m_Z = \frac{m_W}{cos\theta_W}$ in terms of the Weinberg angle θ_W. With $sin^2\theta_W \approx 0.23$, it turns out $m_Z \approx 91$ GeV , matching what was observed. [27]

These vector bosons obtain relatively large masses while the photon γ remains massless, consistent with the conservation of $U(1)_{\text{em}}$. At the same time, the three "absorbed" Goldstone bosons become the longitudinal modes of $W^{\pm}$ and Z^0, completing their 3 polarization degrees

of freedom as massive spin-1 particles.

The Higgs mechanism also explains the mass of fermions by Yukawa couplings. The Higgs field interacts with each mass fermion m_f through a term $y_f \bar{\psi}_L \psi_R H$ (and its conjugates), where y_f is the Yukawa constant. After the symmetry breaking, the Higgs acquires $\langle H \rangle = v/\sqrt{2}$ and generates a mass term $m_f = y_f \frac{v}{\sqrt{2}}$. Thus, the numeric value of y_f is determined by the mass of the fermion. For example, for the electron ($m_e \approx 0.511 MeV$) you get a tiny Yukawa $y_e \sim 3 \times 10^{-6}$, while for the top quark ($m_t \approx 173$ GeV) you require $y_t \sim 1$. This huge hierarchy of Yukawa couplings reflects the mass disparity between light and heavy fermions in the SM [15]. Each fermion interacts with the Higgs field according to its y_f and consequently gains mass by propagating in the Higgs vacuum. Experimentally, these interactions have been confirmed by measuring, for example, the rates of decay of Higgs in pairs of fermions. Decays have been observed to leptons τ ($H \to \tau^+\tau^-$) and quarks b ($H \to b\bar{b}$) consistent with the predicted values of y_τ and y_b, which supports that these masses come from the Higgs mechanism. In contrast, fermions lacking a Yukawa term in the Standard Model - notably neutrinos in the minimal model - would remain massless, which motivates extending the model to explain their small observed masses [21].

Finally, the Higgs boson itself acquires a m_H mass through its own potential. Before the breakup, the potential of the Higgs has the form:

$$V(H) = \mu^2 |H|^2 + \lambda |H|^4 \tag{1.1}$$

With $\mu^2 < 0$ a negative value that spontaneously breaks the symmetry $SU(2)_L \times U(1)_Y$, and $\lambda |H|^4$ is the self-interaction term that stabilizes the potential, giving a global minimum; the field spontaneously develops $v^2 = -\mu^2/\lambda$. The mass of the Higgs results in $m_H^2 = 2\lambda v^2$. For $m_H \approx 125$ GeV, these parameters are determined approximately as $\lambda \sim 0.13$ on the electroweak scale.

It is important to note that the Higgs mechanism in its minimal form does not explain the origin of the mass values themselves but provides a consistent means of introducing them into the theory. The mass of the Higgs boson itself is a free parameter in the SM. Similarly, the SM does not clarify why each fermion has such a disparate coupling (and therefore a mass) this "mass spectrum" from neutrinos to top quark remains an open mystery. Despite these unknowns, the Higgs mechanism is extremely successful because it allows masses to be incorporated into electroweak theory without violating its fundamental symmetries, keeping predictions in accordance with experiments.[25]

1.3 The Higgs Boson in the Standard Model: predictions and properties.

The SM predicts a single Higgs boson with well-defined properties: it is a spin 0 scalar particle, with no electric charge or color, with a mass of $m_H \approx 125$ GeV, and it is its own antiparticle. Before its discovery, it had been experimentally limited that its mass should exceed 114 GeV (lower limit given by the LEP experiment [1]) but not exceeding about 700 GeV. Beyond those limits, the SM would have needed modifications. The concrete mass could not be deduced from the beginning, so it was the subject of experimental research for decades [11]. The decay channels of the Higgs boson could also be predicted once its hypothetical mass was fixed. For example, a light Higgs (around $100 - 140$ GeV) should decay mainly into the heaviest fermions available

(pair of bottom quarks, tau leptons) or into, if kinematically permitted, W or Z bosons, and less likely into photons (via loops of heavy particles). These predictions allowed defining ways to detect a Higgs in detectors, such as pairs of high-momenta photons, signal of $H \to \gamma\gamma$; pairs of leptons from Z, signal of $H \to ZZ^* \to 4$ (The symbol * denotes an off-shell decay in one of the Z bosons because $m_H < 2m_Z$), excess events with pairs of b-quarks, etc. By 2012, experiments had unsuccessfully explored much of the possible mass range, but there was a window around $115 - 130$ GeV where a Higgs could have been "hiding" without being excluded yet [22].

Over the past decade, the LHC ATLAS and CMS experiments have conducted extensive investigations into these channels. The findings consistently indicate that the observed Higgs particle aligns with the predictions of the Standard Model. Given the current uncertainties, which are approximately 10% concerning their couplings, no significant deviations have been observed. The measured production and decay rates are in agreement with theoretical expectations. Notably, in 2018, the predominant decay mode $H \to \bar{b}b$ was corroborated, revealing a statistically significant excess congruent with the anticipated 58% [28]. In the bosonic channels identified in 2012 ($H \to \gamma\gamma, ZZ^*, W^+W^-$), the ATLAS and CMS collaborations have refined the Signal Strength measurements (mu), obtaining values that are in close proximity to $mu = 1$, as predicted for a standard Higgs, across all modes within the errors of $10\% - 15\%$.

The 125 GeV Higgs boson has so far presented properties compatible with the predictions of the SM; it is a scalar particle that couples bosons and fermions with a force proportional to their masses. This remarkable agreement reinforces the validity of the Brout-Englert-Higgs mechanism while imposing restrictions on possible deviations due to new physics. Searches continue in rare modes (e.g. invisible or exotic decays) to check whether the Higgs could also connect with sectors beyond the Standard Model, although there is no indication of this so far.

1.4 Higgs Boson Discovery: Implications for Modern Physics

On 4 July 2012, the LHC ATLAS and CMS experiments announced the observation of a new particle compatible with the SM Higgs boson. Both detectors reported significant excesses of events in the expected decay channels, in particular $H \to \gamma\gamma$ and $H \to 4$, with a combined statistical significance exceeding the 5σ for CMS and 6σ in ATLAS, the threshold required for a discovery. The new particle had a mass around 125 GeV (figure 1.4) [13] [14].

Comprehensive analysis of the production and decay modes of the new boson confirmed that the precise mass was $m_H = 125.09 \pm 0.21(stat.) \pm 0.11(syst.)$ GeV and its spin-parity was determined as $J^p = 0^+$, matching the predictions of the Standard Model (figure 1.3). By 2013, there was no longer any doubt that it was the Higgs boson. This achievement was recognized with the 2013 Nobel Prize in Physics to Peter Higgs and François Englert, for having theoretically anticipated the BEH mechanism and its associated boson decades earlier.
The discovery of the Higgs boson completes the Standard Model as a theoretical framework, enabling us to comprehend the origin of the masses of the W and Z bosons, as well as the fundamental fermions, within the context of field theory. It has been confirmed that the vacuum of our universe is permeated by the Higgs field, and that particles acquire mass through their interaction with this field. This demonstrates that the SM is a self-consistent theory up to very high energies, having successfully passed a crucial test. Notably, the Higgs boson is the first scalar elementary particle to be observed, representing a significant milestone in our understanding of physics. Furthermore, the Higgs boson has implications for cosmological phenomena. The Higgs field may have played a role during the early stages of the universe: the electroweak phase transition could influence phenomena such as matter-antimatter asymmetry. Additionally, there

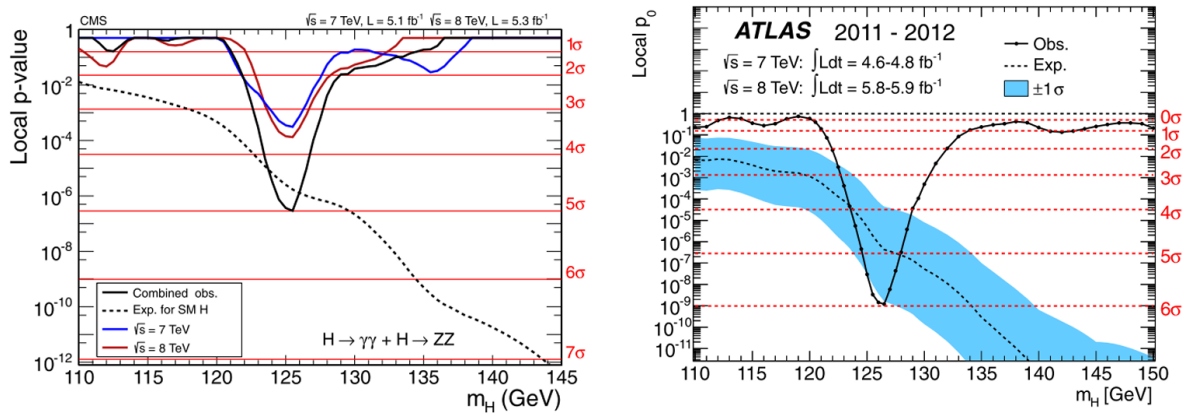

Figure 1.3: (Local p-value versus Higgs-boson mass for the $H \to \gamma\gamma$ and $H \to ZZ$ channels as measured by CMS (left)[14] and ATLAS (Right)[13]; both datasets exhibit minima near $m_H \approx 125$ GeV, consistent with the discovery significance.

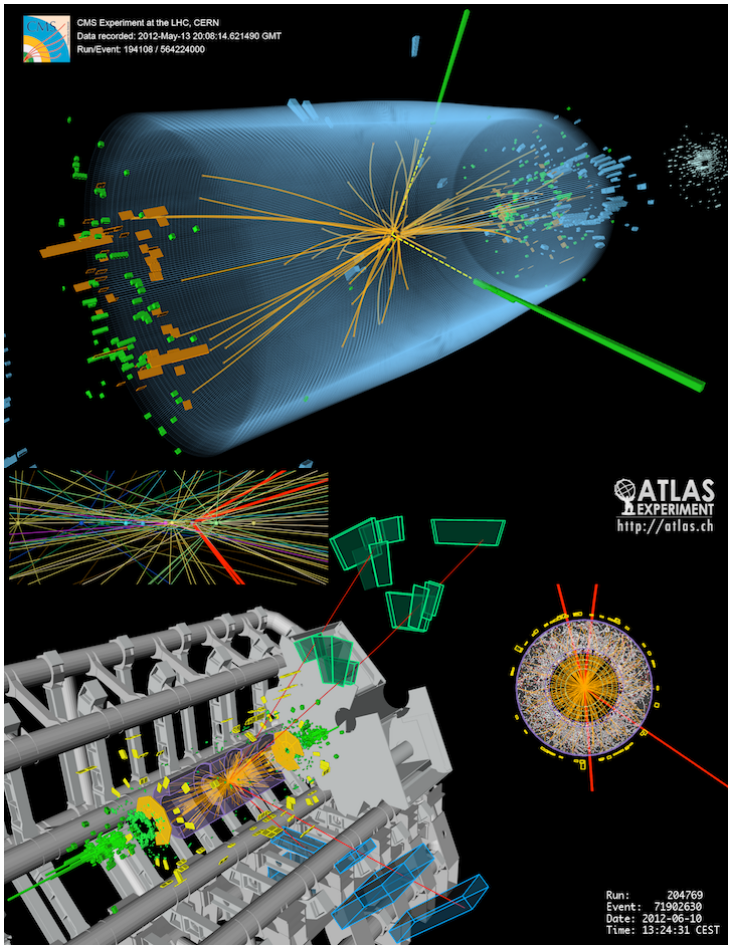

Figure 1.4: Example candidate events recorded in 2012: a diphoton final state in CMS (Above) and a four-muon final state in ATLAS (Down)

is explored whether the Higgs can serve as a "portal" to hidden sectors such as dark matter. Extended models suggest that the Higgs could interact weakly with dark matter particles, implying that a detailed study of the Higgs in detail could reveal clues to those invisible entities.

The discovery of the Higgs boson at 125 GeV validated the SM, but simultaneously opened up questions about the possible existence of other as yet unobserved scalar states. Subsequent reports from the ATLAS and CMS experiments have suggested anomalies at lower masses, particularly around 95 GeV. These anomalies motivate the theoretical and experimental exploration of scenarios with lighter additional Higgs bosons, predicted by models such as Georgi-Machacek, S2HDM, or CP-violated models. Exploring these scenarios is crucial not only to understand the full structure of the Higgs mechanism, but also to investigate possible windows to physics Beyond the Standard Model (BSM).

1.5 Experimental Hints for Light Scalars.

The discovery of the 125 GeV Higgs boson in 2012 completed the minimal Higgs sector of the SM. Yet many theoretical frameworks suggest that this Higgs is not alone. Numerous beyond-the-SM (BSM) models predict the existence of several Higgs bosons, at least one of which could be lighter than 125 GeV. Finding a second Higgs boson would indicate that the Higgs field's role in giving masses to particles is more complex than in the SM, and would be an unequivocal sign of new physics. There are strong motivations to search for such additional light Higgs bosons [12].

Higgs bosons with masses below 125 GeV have been actively searched for at the Large Electron-Positron Collider (LEP) [1], Tevatron, and the Large Hadron Collider (LHC). No second Higgs has been confirmed, but intriguing small excesses have appeared. In particular, the CMS experiment has reported excess events near 95 GeV in the di-photon ($H \to \gamma\gamma$) channel (local significance ~ 2.8–2.9σ).[4][7], and recently in the di-τ channel ($H \to \tau^+\tau^-$) (local significance $\sim 3.1\sigma$).There is also a longstanding $\sim 2.3\sigma$ excess in $e^+e^- \to ZH$ with $H \to b\bar{b}$ at LEP around $95-100$ GeV [6]. (A deeper discussion of its phenomenological implications is developed in the Chapter 2 devoted to BSM analysis.) The possible existence of a second, lighter Higgs boson motivates the continuation of searches at the LHC and future colliders, since even a subtle signal could announce new physics.

T.D. Lee originally introduced a two-Higgs-doublet model in 1973 as a mechanism for enabling spontaneous CP violation within the Higgs sector. Models incorporating CP-violating Higgs fields have the potential to provide sufficient CP asymmetry required for baryogenesis. Specifically, if the Lagrangian remains CP-invariant while the vacuum does not, considerations of perturbativity indicate that not all additional Higgs states can assume significantly large masses; one charged boson and two neutral bosons must be positioned near the electroweak scale. This scenario renders the presence of relatively light additional scalars as natural rather than excessively fine-tuned [24]. An examination of three conceptually robust Beyond Standard Model (BSM) Higgs sector models is presented, all predicting supplementary scalar bosons that could potentially elucidate a 95 GeV Higgs candidate in the diphoton, $b\bar{b}$, and $\tau^+\tau^-$ channels: the Georgi–Machacek model, the Two-Higgs-Doublet Model, and the Higgs Singlet Model.

The Georgi–Machacek model, proposed in 1985 by Howard Georgi and Mary Machacek, extends the SM Higgs sector by adding two $SU(2)_L$ triplet scalar fields in such a way that custodial symmetry is preserved. This custodial $SU(2)$ ensures the electroweak ρ-parameter remains $\rho = 1$ at tree-level [8], avoiding conflicts with precision measurements.

The GM model predicts five physical Higgs states beyond the 125 GeV Higgs. These form custodial-symmetry multiplets: a custodial five-plet ($H_5^{\pm\pm}, H_5^{\pm}, H_5^0$), a custodial triplet

$(H_3^{\pm}, H_3^0)$, and a custodial singlet H_1^0. The custodial-5plet includes a doubly-charged Higgs $H_5^{\pm\pm}$, a singly-charged $H_5^{\pm}$, and a neutral H_5^0, all nearly degenerate in mass at tree-level due to the symmetry. The custodial-singlet H_1^0 corresponds to a combination of the doublet and triplet neutral fields. The 125 GeV Higgs can be identified with the custodial-singlet H_1^0, which is predominantly the doublet field (ensuring its couplings match the SM Higgs). This leaves the triplet-derived states free to be lighter [8].

The Two-Higgs-Doublet Model (2HDM) is a well-studied extension of the Standard Model (SM) that introduces a second scalar doublet, resulting in five physical Higgs bosons: two CP-even (h, H with $m_h < m_H$), one neutral CP-odd (A), and two charged (H^+, H^-). This extended scalar sector allows for rich phenomenology, including the possibility of a light Higgs boson around 95 GeV, which has garnered interest due to observed excesses in experimental data [23][8][18]. The canonical 2HDM provides the framework and motivation, as additional scalars and potential new CP phases to consider a ~ 95 GeV Higgs candidate. This has led to the exploration of extensions or variations of the 2HDM that offer more freedom to realize a 95 GeV Higgs while satisfying experimental constraints [5].

The Higgs Singlet Model (HSM) is an extension of the SM Higgs sector, consisting of adding a single new real scalar field S that is a singlet under the SM gauge groups. It retains the SM Higgs doublet Φ and introduces S which mixes with the Higgs field after electroweak symmetry breaking. The HSM serves as a simple benchmark for theories with an extra neutral scalar and is frequently used to guide experimental searches, due to its minimality and few parameters.

Because of its simplicity, the HSM is often used by experimental collaborations as a benchmark for low-mass Higgs searches. Limits and excesses can be reinterpreted in terms of the $\sin^2\alpha$ vs M_{H_1} parameter space. For instance, ATLAS and CMS have set upper limits on $\sin^2\alpha$ as a function of a second Higgs mass from 1 GeV up to several hundred GeV [26][6].

Chapter 2

Experimental Evidence and Phenomenological Treatment

Effective Interactions and Decay Channels

The ATLAS and CMS collaborations employ the Signal Strength (μ) to assess the observed data align with Standard Model (SM) expectations in different decay channels. This parameter is characterized as the ratio of the observed Branching Ratio of particle production ($\mathcal{B}^{obs}(X \to 1,2)$) to its theoretical prediction ($\mathcal{B}^{theo}(X \to 1,2)$), multiplied by the ratio of the observed Cross-Section for the production channel ($\sigma^{obs}(3,4 \to X)$) to the corresponding theoretical Cross-Section ($\sigma^{theo}(3,4 \to X)$).We contemplate the introduction of a new hypothetical scalar boson, referred to as ϕ, which possesses the same quantum numbers (spin, charge) and production/decay mechanisms as those of the SM Higgs boson, but with an assigned mass of 95.4 GeV. The Signal Strength is formally defined as

$$\mu_{\gamma\gamma,\tau\tau} = \frac{\sigma^{obs}(gg \to \phi \to \gamma\gamma, \tau^+\tau^-)}{\sigma^{theo}(gg \to \phi \to \gamma\gamma, \tau^+\tau^-)} \approx \frac{\mathcal{B}^{obs}(\phi \to \gamma\gamma, \tau^+\tau^-)\sigma^{obs}(gg \to \phi)}{\mathcal{B}^{theo}(\phi \to \gamma\gamma, \tau^+\tau^-)\sigma^{theo}(gg \to \phi)}. \tag{2.1}$$

The Signal Strength of the $\phi \to \bar{b}b$ decay can be differentiated from the $\phi \to \gamma\gamma, \tau^+\tau^-$ decays based on the production channel. As is exposed in the preceding Chapter (1.5), the LEP indicated the presence of a lighter Higgs boson within the $e^+e^- \to ZH(H \to \bar{b}b)$ interaction. Therefore, the Signal Strength for this decay is

$$\mu_{bb} = \frac{\sigma^{obs}(e^+e^- \to Z\bar{b}b)}{\sigma^{theo}(e^+e^- \to Z\bar{b}b)} \approx \frac{\sigma^{obs}(e^+e^- \to Z)\mathcal{B}^{obs}(Z \to \phi Z)\mathcal{B}^{obs}(\phi \to \bar{b}b)}{\sigma^{theo}(e^+e^- \to Z)\mathcal{B}^{theo}(Z \to \phi Z)\mathcal{B}^{theo}(\phi \to \bar{b}b)}. \tag{2.2}$$

Given the emphasis on the lighter Higgs boson (ϕ), it is appropriate to equate the theoretical and observed cross-sections in equation 2.2. This results in

$$\mu_{bb} = \frac{\mathcal{B}^{obs}(Z \to \phi Z)\mathcal{B}^{obs}(\phi \to \bar{b}b)}{\mathcal{B}^{theo}(Z \to \phi Z)\mathcal{B}^{theo}(\phi \to \bar{b}b)}. \tag{2.3}$$

The branching ratio is defined in terms of the Partial Decay Width and the Total Width, the latter being the cumulative sum of all kinematically permissible Partial Decay Widths:

$$\mathcal{B}(\phi \to 1,2) = \frac{\Gamma_{\phi \to 1,2}}{\Gamma_{tot}} = \frac{\Gamma_{\phi \to 1,2}}{\sum_i \Gamma_{\phi \to i}}. \tag{2.4}$$

By using the relevant Feynman rules to compute the squared amplitude ($|\mathcal{M}|^2$), the decay width is subsequently determined through Fermi's Golden Rule,

$$\Gamma = \frac{S|\mathbf{p}|}{8\pi m_1^2}|\mathcal{M}|^2; \tag{2.5}$$

here, $S = \frac{1}{n}$ represents the symmetry term for n identical particles in the final state, $|\mathbf{p}| = \frac{1}{2m_1}\sqrt{m_1^4 + m_2^4 + m_3^4 - 2m_1^2m_2^2 - 2m_1^2m_3^2 - 2m_2^2m_3^2}$ signifies the magnitude of either outgoing momentum in terms of the mass of the initial state particle (m_1), and the masses of the two particles in the final state (m_2, m_3); while $\mathcal{M}$ denotes the amplitude matrix, which contains the full information about the interaction vertex. This value is accessible through the Feynman Rules [17].

As discussed in Section 1.5, the ATLAS and CMS experiments have reported an observed excess corresponding to a mass of 95.4 GeV in the di-photon channel, quantified in terms of a signal strength of [3]

$$\mu_{\gamma\gamma}^{exp} = 0.24^{+0.09}_{-0.08}, \tag{2.6}$$

additionally, the CMS experiment observed an excess at around 100 GeV, showing a significance of 3.1σ in the $pp \to H \to \tau^+\tau^-$ channel. This observation suggests that a significance of 2.6σ is consistent with a mass of 95.4 GeV. Consequently, the signal strength at 95 GeV is

$$\mu_{\tau\tau}^{exp} = 1.2 \pm 0.5. \tag{2.7}$$

The LEP experiment documented an excess of 2.3σ in the $e^+e^- \to ZH(H \to b\bar{b})$ decay channel, aligning with a Higgs boson mass of 95.4 GeV, which corresponds to $m_\phi = 95.4$ GeV. The signal strength reported for the $H \to b\bar{b}$ decay is

$$\mu_{bb}^{exp} = 0.117 \pm 0.057. \tag{2.8}$$

With available signal strength values for the $\phi \to \gamma\gamma$, $\phi \to \tau^+\tau^-$, and $\phi \to b\bar{b}$ channels, the next objective is to compute the amplitude matrix for each interaction by defining their respective Lagrangian densities and employing the Feynman rules.

2.1 The decay $\phi \to \gamma\gamma$

The Lagrangian corresponding to the $\phi \to \gamma\gamma$ interaction can be articulated using the Hagiwara basis. The Hagiwara basis constitutes a parametrization employed within the realm of particle physics to describe anomalous interactions between the Higgs boson and other gauge bosons, such as the Z and γ bosons. This parametrization was initially introduced in the K. Hagiwara paper and others in 1993 [16], wherein form factors h_i were proposed to characterize deviations from the Standard Model at the vertices HZZ,$HZ\gamma$, and $H\gamma\gamma$, by incorporating possible effects arising from new physics. For instance, in the context of the $H \to ZZ$ decay, the Lagrangian is defined as,

$$\begin{aligned}\mathcal{L}_{HZZ} =& \frac{g}{c_W}m_Z[\frac{(1-a_Z)}{2}HZ^\mu Z_\mu + \frac{1}{2m_Z^2}(\hat{b}_Z HZ^{\mu\nu}Z_{\mu\nu} \\ &+ \hat{c}_Z HZ^\mu\partial^\nu Z_{\mu\nu} + \tilde{b}_Z HZ^{\mu\nu}\tilde{Z}_{\mu\nu})];\end{aligned} \tag{2.9}$$

where $Z_{\mu\nu} = \partial_\mu Z_\nu - \partial_\nu Z_\mu$ denotes the Z-boson field tensor and its corresponding dual is $\tilde{Z}_{\mu\nu}$; $\hat{a}_Z$ stands for the standard coupling of the Higgs with the Z bosons, with $\hat{b}_Z$ and $\hat{c}_Z$ being the CP-conserving form factors, while $\tilde{b}_Z$ represents the CP-violating form factor [19]. The relationship

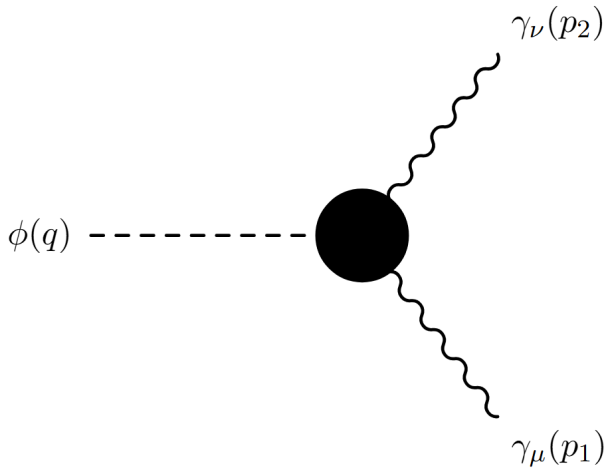

Figure 2.1: Feynman diagram of the $\phi \to \gamma\gamma$ interaction

between these parameters and the form factors h_i is expressed explicitly as:

$$\begin{aligned} h_1^V(q^2, p_1^2, p_2^2) &= 1 + a_Z - \hat{b}_Z \frac{q^2 - p_1^2 - p_2^2}{m_Z^2} + \frac{\hat{c}_Z}{2} \frac{p_1^2 + p_2^2}{m_Z^2} \\ h_2^V(q^2, p_1^2, p_2^2) &= \pm 2\hat{b}_Z \\ h_3^V(q^2, p_1^2, p_2^2) &= \pm 2\tilde{b}_Z \end{aligned} \tag{2.10}$$

, where h_1 denotes the scalar term (CP-conserving), which within the Standard Model assumes the value of $h_1 = 1$; h_2 pertains to a CP-conserving term, induced at the loop level and generally considered small within the Standard Model. Lastly, h_3 represents the CP-violating term, which is of particular interest as it could signify the presence of physics BSM.

The effective Lagrangian $\phi\gamma\gamma$ (Figure 2.1) resembles the HZZ interaction (equation 2.9), with notable differences: since the Higgs field does not couple directly to photons, the decay channel $\phi \to \gamma\gamma$ is not allowed at tree-level within the SM; so there is no $\phi A^\mu A_\mu$ term in the Lagrangian. However, decay $\phi \to \gamma\gamma$ happens through charged particle loops. The effective Lagrangian for the $\phi \to \gamma\gamma$ interaction is given by:

$$\mathcal{L}_{\phi\gamma\gamma} = \frac{g_w}{2m_\phi}(\hat{b}_\gamma \phi A^{\mu\nu} A_{\mu\nu} + \tilde{b}_\gamma \phi A_{\mu\nu} \tilde{A}^{\mu\nu}) \tag{2.11}$$

In this context, $A_{\mu\nu} = \partial_\mu A_\nu - \partial_\nu A_\mu$ denotes the photon field tensor, whereas $\tilde{A}_{\mu\nu}$ represents its dual space. The factors $\hat{b}_\gamma$, $\hat{c}_\gamma$ are CP-conserving factors and $\tilde{b}_\gamma$ is the CP-violating factor. Furthermore, q is the four-momentum of the **hypothetical new Higgs** ϕ, p_i are four-momenta of the outgoing photons, considering that $p_i^2 = m_\gamma^2 = 0$ and $m_Z^2 \to m_\phi^2 = q^2$ because the hypothetical light Higgs boson (ϕ) is the only particle that contributes mass to the interaction. The form factors defined in the equation 2.10 result:

$$\begin{aligned} h_1^{\gamma\gamma}(q^2, p_1^2, p_2^2) &= -\hat{b}_\gamma, \\ h_2^{\gamma\gamma}(q^2, p_1^2, p_2^2) &= \pm 2\hat{b}_\gamma, \\ h_3^{\gamma\gamma}(q^2, p_1^2, p_2^2) &= \pm 2\tilde{b}_\gamma. \end{aligned} \tag{2.12}$$

The constructed Lagrangian comprehensively characterizes the interaction, incorporating form factors that reflect potential physics beyond the Standard Model. To derive the vertex factor, Wolfram Mathematica serves as an instrumental utility for defining the Lagrangian [2][9].

The Lagrangian configurations in Mathematica adhere to the references $T_1 \equiv \hat{b}_\gamma \phi A^{\mu\nu} A_{\mu\nu}$, $T_2 \equiv \tilde{b}_\gamma \phi A_{\mu\nu} \tilde{A}^{\mu\nu}$, where $A_{til} \equiv \tilde{A}^{\mu\nu} = \frac{1}{2}\epsilon^{\mu\nu\alpha\beta} A_{\alpha\beta}$. Subsequently, acquiring the vertex factor requires the employment of the command FeynmanRules executed on the Lagrangian as delineated in Listing 2.1.

```
(*Writing the Lagrangian term by term (Ti)*)
(*Working with FeynRules*)
A_til = 1/2 Eps[μ, ν, α, β] FS[A, α, β];
T1 = by phi FS[A, μ, ν] FS[A, μ, ν];
T2 = by phi FS[A, μ, ν] A_til;

(* Writing the Lagrangian*)
LHγγ = gw ((1/(2 Mphi)) (T1 + T2))

(*Obtaining the vertex factor*)
Vertex = FeynmanRules[LHγγ]
```

Listing 2.1: $\phi\gamma\gamma$ Lagrangian definition in Mathematica

This command yields the vertex factor expressed in terms of $\hat{b}_\gamma$, $\hat{c}_\gamma$, and $\tilde{b}_\gamma$. However, considering the specification of the form factors as outlined in equation 2.12, we derive:

$$V^{\mu\nu}_{\phi\gamma\gamma} \equiv ig\Gamma^{\mu\nu}_{\phi\gamma\gamma}, \tag{2.13}$$

where $\Gamma^{\mu\nu}_{\phi\gamma\gamma} = h_1^{\gamma\gamma} g^{\mu\nu} m_\phi + \frac{1}{m_\phi}\{h_2^{\gamma\gamma} p_1^\nu p_2^\mu + h_3^{\gamma\gamma} \epsilon^{\mu\nu\alpha\beta} p_{1\alpha} p_{2\beta}\}$ [19].

According to the Feynman Rules corresponding to the diagram illustrated in figure 2.1, where the outgoing photons impart the factors $\epsilon^{\mu*}(p_1, \lambda_1)$ and $\epsilon^{\nu*}(p_2, \lambda_2)$, and the **light Higgs boson** does not contribute any factor beyond the vertex 2.13, the resultant amplitude matrix and its squared modulus are given by:

$$i\mathcal{M} = ig\epsilon^{\mu*}(p_1, \lambda_1)\epsilon^{\nu*}(p_2, \lambda_2)[h_1^{\gamma\gamma} m_\phi g_{\mu\nu} + \frac{1}{m_\phi}\{h_2^{\gamma\gamma} p_{1\nu} p_{2\mu} + h_3^{\gamma\gamma} \epsilon_{\mu\nu\alpha\beta} p_1^\alpha p_2^\beta\}] \tag{2.14}$$

$$\begin{aligned} \rightarrow |\mathcal{M}|^2 =& g^2 \Sigma_{\lambda_1} \epsilon^{\mu*}(p_1, \lambda_1)\epsilon^{\sigma}(p_1, \lambda_1) \Sigma_{\lambda_2} \epsilon^{\nu*}(p_2, \lambda_2)\epsilon^{\delta}(p_2, \lambda_2) \\ & \times [h_1^{\gamma\gamma} m_\phi g_{\mu\nu} + \frac{1}{m_\phi}\{h_2^{\gamma\gamma} p_{1\nu} p_{2\mu} + h_3^{\gamma\gamma} \epsilon_{\mu\nu\alpha\beta} p_1^\alpha p_2^\beta\}] \\ & \times [h_1^{\gamma\gamma*} m_\phi g_{\sigma\delta} + \frac{1}{m_\phi}\{h_2^{\gamma\gamma*} p_{1\delta} p_{2\sigma} + h_3^{\gamma\gamma*} \epsilon_{\sigma\delta\theta\tau} p_1^\theta p_2^\tau\}] \end{aligned} \tag{2.15}$$

, where the sum over polarizations is performed: $\Sigma_\lambda \epsilon^{\mu*}(p, \lambda)\epsilon^{\nu}(p, \lambda) = -g^{\mu\nu}$ (for photons). Typically, collider experiments do not measure explicitly the polarization states (or intrinsic spins, see subsection 2.2) of final-state particles. Therefore, summing over polarizations ensures that the resulting expression provides observable quantities independent of polarization.

$$\begin{aligned} \rightarrow |\mathcal{M}|^2 =& g^2 (g^{\mu\sigma} g^{\nu\delta} [h_1^{\gamma\gamma} m_\phi g_{\mu\nu} + \frac{1}{m_\phi}\{h_2^{\gamma\gamma} p_{1\nu} p_{2\mu} + h_3^{\gamma\gamma} \epsilon_{\mu\nu\alpha\beta} p_1^\alpha p_2^\beta\}] \\ & \times [h_1^{\gamma\gamma*} m_\phi g_{\sigma\delta} + \frac{1}{m_\phi}\{h_2^{\gamma\gamma*} p_{1\delta} p_{2\sigma} + h_3^{\gamma\gamma*} \epsilon_{\sigma\delta\theta\tau} p_1^\theta p_2^\tau\}]). \end{aligned} \tag{2.16}$$

Carrying out the contraction of the Lorentz indices and using standard Levi-Civita tensor properties ($\epsilon^{\mu}_{\ \mu\alpha\beta} = 0$, $\epsilon_{\mu\nu\alpha\beta}\epsilon^{\mu\nu\sigma\rho} = (\delta^{\sigma}_{\alpha}\delta^{\rho}_{\beta} - \delta^{\rho}_{\alpha}\delta^{\sigma}_{\beta})$), we arrive at the simplified expression:

$$\to |\mathcal{M}|^2 = g^2 m_\phi^2 (4|h_1^{\gamma\gamma}|^2 + \frac{1}{2}h_1^{\gamma\gamma}h_2^{\gamma\gamma *} + \frac{1}{2}h_1^{\gamma\gamma *}h_2^{\gamma\gamma} + \frac{1}{2}|h_3^{\gamma\gamma}|^2) \tag{2.17}$$

Owing to gauge invariance at vertex 2.13, it is imperative for $p_{1\mu}$ that the Ward identity on the vertex factor be satisfied,

$$0 = p_{1\mu} i g \Gamma^{\mu\nu}_{\phi\gamma\gamma}. \tag{2.18}$$

Given that i represents the complex unit and $g \neq 0$, consequently leading to,

$$\begin{aligned} 0 &= p_{1\mu}(h_1^{\gamma\gamma} m_\phi g^{\mu\nu} + \frac{1}{m_\phi}\{h_2^{\gamma\gamma} p_1^\nu p_2^\mu + h_3^{\gamma\gamma}\epsilon^{\mu\nu\alpha\beta} p_{1\alpha} p_{2\beta}\}) \\ &= h_1^{\gamma\gamma} m_\phi p_1^\nu + \frac{1}{m_\phi} h_2^{\gamma\gamma} p_1^\nu (p_{1\mu} p_2^\mu) + \frac{1}{m_\phi} h_3^{\gamma\gamma}\epsilon^{\mu\nu\alpha\beta} p_{1\mu} p_{1\alpha} p_{2\beta}\}. \end{aligned} \tag{2.19}$$

In the context of the term associated with $h_3^{\gamma\gamma}$, it is recognized that $p_{1\mu}p_{1\alpha} = p_{1\alpha}p_{1\mu}$ can be commuted, and due to the properties of the Levi-Civita symbol, $\epsilon^{\mu\nu\alpha\beta} = -\epsilon^{\alpha\nu\mu\beta}$ anticommutes. This results in the relation

$$\epsilon^{\mu\nu\alpha\beta} p_{1\mu} p_{1\alpha} = -\epsilon^{\alpha\nu\mu\beta} p_{1\alpha} p_{1\mu}. \tag{2.20}$$

By renaming the summation index on the right side of the equation ($\mu \to \alpha$ and $\alpha \to \mu$), the expression

$$\epsilon^{\mu\nu\alpha\beta} p_{1\mu} p_{1\alpha} = -\epsilon^{\mu\nu\alpha\beta} p_{1\mu} p_{1\alpha}, \tag{2.21}$$

is equivalent to its negative, thus $\epsilon^{\mu\nu\alpha\beta} p_{1\mu} p_{1\alpha} = 0$. Considering this, in conjunction with $p_{1\mu}p_2^\mu = \frac{m_\phi^2}{2}$, yields the derivation of

$$(h_1^{\gamma\gamma} + \frac{1}{2}h_2^{\gamma\gamma}) p_1^\nu m_\phi = 0. \tag{2.22}$$

As both p_1^ν and m_ϕ are required to be non-null, therefore,

$$h_1^{\gamma\gamma} + \frac{1}{2}h_2^{\gamma\gamma} = 0 \to h_2^{\gamma\gamma} = -2h_1^{\gamma\gamma}. \tag{2.23}$$

A similar relation applies for $p_{2\nu}$, and the procedure mirrors that for $p_{1\mu}$. We can replace $h_2^{\gamma\gamma} = -2h_1^{\gamma\gamma}$ in the equation 2.17, which ultimately leads to

$$|\mathcal{M}|^2 = \frac{g^2 m_\phi^2}{2}(4|h_1^{\gamma\gamma}|^2 + |h_3^{\gamma\gamma}|^2). \tag{2.24}$$

The next step is to calculate the Decay Width following Fermi's Golden Rule defined in equation 2.5, taking $S = \frac{1}{2}$ for two photons in the final state, $|\mathbf{p}| = \frac{m_\phi}{2}$ for $m_1 = m_\phi$ and $m_2 = m_3 = 0$, and the modulus of the amplitude matrix (eq. 2.24), thus the Partial Decay Width of the interaction is:

$$\Gamma_{\phi\to\gamma\gamma} = \frac{g^2 m_\phi^2 (4|h_1^{\gamma\gamma}|^2 + |h_3^{\gamma\gamma}|^2)}{64\pi}, \tag{2.25}$$

this is the Partial Decay Width in its general form, but considering that ϕ is being modeled as a Higgs boson at a mass of 95.4 GeV and that in the SM, the factor $h_3^{\gamma\gamma} = 0$, because CP violation is not considered; the expression of the Decay Width within the theory results

$$\Gamma^{theo}_{\phi\to\gamma\gamma} = \frac{g^2 m_\phi |h^{\gamma\gamma}_{1(theo)}|^2}{16\pi}, \tag{2.26}$$

which leads to the definition of the theoretical Branching Ratio:

$$\mathcal{B}^{theo}(\phi\to\gamma\gamma) = \frac{\Gamma^{theo}_{\phi\to\gamma\gamma}}{\Gamma^{theo}_{\phi,Tot}} = \frac{g^2 m_\phi |h^{\phi\gamma\gamma}_{1(theo)}|^2}{16\pi\Gamma^{theo}_{\phi,Tot}}, \tag{2.27}$$

and taking the Partial Decay Width in its general form (eq. 2.25) to build the expression of the observed Branching Ratio:

$$\mathcal{B}^{obs}(\phi\to\gamma\gamma) = \frac{\Gamma_{\phi\to\gamma\gamma}}{\Gamma^{obs}_{\phi,Tot}} = \frac{g^2 m_\phi (|4h_1^{\gamma\gamma}|^2 + |h_3^{\gamma\gamma}|^2)}{64\pi\Gamma^{obs}_{\phi,Tot}}, \tag{2.28}$$

the expression of the Signal Strength of the $\phi\gamma\gamma$ interaction results

$$\mu_{\gamma\gamma} = \frac{\mathcal{B}^{obs}(\phi\to\gamma\gamma)\sigma^{obs}(gg\to\phi)}{\mathcal{B}^{theo}(\phi\to\gamma\gamma)\sigma^{theo}(gg\to\phi)} = \frac{4|h_1^{\phi\gamma\gamma}|^2 + |h_3^{\phi\gamma\gamma}|^2}{4|h^{\gamma\gamma}_{1(theo)}|^2}\kappa^2, \tag{2.29}$$

If the amplitude of production channel $gg\to\phi$ is modified only by a multiplicative real constant factor κ^2 applied to the entire theoretical amplitude, the Cross-Section consequently undergoes scaling by a factor of κ^2. This parameter serves as a model of the behavior of the Signal Strength (equation 2.29) under the influence of Beyond Standard Model (BSM) physics originating from the production channel. Considerations of $\Gamma^{obs}_{\phi,Tot} \simeq \Gamma^{theo}_{\phi,Tot}$ and $h^{\gamma\gamma}_{1(theo)} = 0.201134$ are included.

With this expression, the comparison is made with the results measured in CMS and ATLAS (equation 2.6), so we can graph the allowed values for $h_1^{\gamma\gamma}$ and $h_3^{\gamma\gamma}$ following the restrictions imposed by experimental measurements (see chapter 3).

2.2 The $\phi\to\tau\tau$ and $\phi\to bb$ decays

Within the SM, the coupling of the Higgs boson to a fermion f with mass m_f is exclusively scalar, as dictated by the Yukawa Lagrangian: $\mathcal{L}_{Yuk} = -g\bar{f}fH$. In analyzing the decay processes of the scalar boson ϕ into a fermion-antifermion pair, the interaction can be articulated through a Lagrangian that explicitly differentiates scalar from pseudoscalar couplings. In this context, g_s represents the scalar component ($CP-even$), while g_p denotes the pseudoscalar component ($CP-odd$). The latter is particularly interesting due to its association with CP violation. In the framework of the SM, $g_p = 0$, given that CP violation is not inherently accounted for.

Our starting point is the fermionic one-loop Lagrangian describing the $h_3^{z\gamma}$ contributions to the $HZ\gamma$ interaction detailed in [20],

$$\mathcal{L}_{HZ\gamma} = \frac{g_w}{c_W}\bar{f}_i(g_V^{ij} - g_A^{ij}\gamma^5)f_j Z^\mu + \frac{g_w}{2m_W}\bar{f}_i(g_s^{ij} + g_p^{ij}\gamma^5)f_j H, \tag{2.30}$$

and considering exclusively the interaction term between fermions while transitioning from the SM Higgs boson (H) to the proposed scalar boson (ϕ), this scenario is reduced to a fermion-antifermion pair of the identical flavor to examine the $\phi\to\tau^+\tau^-$ and $\phi\to\bar{b}b$ decays. The resulting Lagrangian of the $\phi\to\bar{f}f$ interaction is presented in

$$\mathcal{L}_{\phi f\bar{f}} = \frac{g_w}{2m_W}\bar{f}(g_s + g_p\gamma^5)f\phi. \tag{2.31}$$

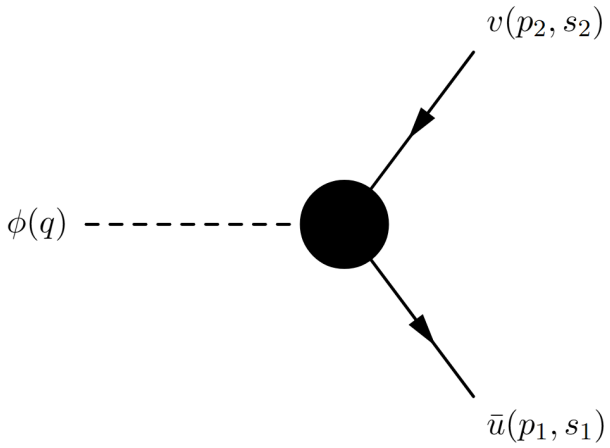

Figure 2.2: Feynman diagram of the $\phi \to ff$ interaction

.

In this context, f and $\bar{f}$ denote the fermion field and its corresponding antifermion, whereas g_s and g_p represent their respective scalar and pseudoscalar couplings, along with the Dirac matrix $\gamma^5 = i\gamma^0\gamma^1\gamma^2\gamma^3$. g_w is the electroweak coupling and m_W the mass of the W boson. Defining the Lagrangian interaction using Wolfram Mathematica:

```
(*Working with FeynRules*)
(* Writing the Lagrangian*)
LHff= gw (1/(2mW))fbar(gs+gp Ga[5]) f phi
```

Listing 2.2: $\phi f \bar{f}$ Lagrangian definition in Mathematica

Within the Mathematica implementation f and $fbar$ represent the fermion-antifermion fields, such as b, $\bar{b}$ or τ^+, τ^-, while the Dirac Matrix γ^5 is denoted by Ga[5]. Similar to the $\phi\gamma\gamma$ decay, to acquire the vertex factor, the command FeynmanRules needs to be applied to the Lagrangian 2.31 (see Listing 2.2 in the previous subsection). The vertex factor results

$$V_{\phi\bar{f}f} = \frac{ig_w}{2m_W}(g_s + g_p\gamma^5). \tag{2.32}$$

The Feynman Rules, following the Feynman diagram in Figure 2.2 where the outgoing fermion imparts the factor $\bar{u}(p_1, s_1)$, and the antifermion the factor $v(p_2, s_2)$. As in the $\phi\gamma\gamma$ decay, the **light Higgs boson** does not contribute any factor, so that the amplitude matrix and its squared modulus result:

$$i\mathcal{M} = \frac{ig_w}{2m_W}\bar{u}(p_1, s_1)(g_s + g_p\gamma^5)v(p_2, s_2) \tag{2.33}$$

$$\to |\mathcal{M}|^2 = \frac{{g_w}^2}{4m_W^2}\Sigma_{s_1}\Sigma_{s_2}\bar{u}(p_1, s_1)(g_s + g_p\gamma^5)v(p_2, s_2)\bar{v}(p_2, s_2)(g_s - g_p\gamma^5)u(p_1, s_1) \tag{2.34}$$

Where the fermion spin sum: $\Sigma_s\bar{u}(p, s)u(p, s) = Tr[\not{p} + m]$, $\Sigma_s\bar{v}(p, s)v(p, s) = Tr[\not{p} - m]$ is used. It is important to acknowledge $\not{p} = \gamma^\mu p_\mu$.

$$|\mathcal{M}|^2 = \frac{g^2}{4m_W^2}Tr[(\not{p}_1 + m_f)(g_s + g_p\gamma^5)(\not{p}_2 - m_f)(g_s - g_p\gamma^5)]. \tag{2.35}$$

Expanding by all the terms in the trace

$$\begin{aligned} Tr[(\not{p}_1 + m_f)(g_s + g_p\gamma^5)(\not{p}_2 - m_f)(g_s - g_p\gamma^5)] &= g_s^2 Tr[(\not{p}_1 + m_f)(\not{p}_2 - m_f)] \\ &+ g_s g_p Tr[(\not{p}_1 + m_f)\gamma^5(\not{p}_2 - m_f)] \\ &- g_s g_p Tr[(\not{p}_1 + m_f)(\not{p}_2 - m_f)\gamma^5] \\ &- g_p^2 Tr[(\not{p}_1 + m_f)\gamma^5(\not{p}_2 - m_f)\gamma^5] \end{aligned} \tag{2.36}$$

Utilizing the trace property $Tr[(\not{p}_1 + m_f)(\not{p}_2 \pm m_f)] = 4(p_1.p_2 \pm m_f^2)$, and the subsequent properties of the γ^5 Dirac matrix: specifically, properties $(\gamma^5)^2 = 1$, $(\gamma^5)^\dagger = \gamma^5$, $\{\gamma^5, \gamma^\mu\} = 0$, and $Tr[n\ odd\ number\ of\ \gamma] = 0$.

$$\begin{aligned} Tr[(\not{p}_1 + m_f)(g_s + g_p\gamma^5)(\not{p}_2 - m_f)(g_s - g_p\gamma^5)] &= 4g_s^2(p_1.p_2 - m_f^2) \\ &+ 4g_p^2(p_1.p_2 + m_f^2) \end{aligned} \tag{2.37}$$

To ensure the conservation of momentum and energy, the system must adhere to the conditions outlined in $q^2 = m_\phi^2 = (p_1 + p_2)^2 = 2p_1.p_2 + 2m_f^2$, which consequently results in $p_1.p_2 = \frac{1}{2}m_\phi^2 - m_f^2$.

$$\rightarrow |\mathcal{M}|^2 = \frac{g_w^2}{2m_W^2}(g_s^2(m_\phi^2 - 4m_f^2) + g_p^2 m_\phi^2) \tag{2.38}$$

Subsequent to the computation of the amplitude matrix, the decay width is determined in accordance with the golden rule of decays (eq. 2.5), taking $S = 1$ for any identical particles in the final state, $|\mathbf{p}| = \frac{1}{2}\sqrt{m_\phi^2 - 4m_f^2}$ for $m_1 = m_\phi$ and $m_2 = m_3 = m_f$; the Partial Decay Width of the $\phi f \bar{f}$ decay results:

$$\Gamma_{\phi\rightarrow\bar{f}f} = \frac{g_w^2\sqrt{m_\phi^2 - 4m_f^2}(g_p^2 m_\phi^2 + g_s^2(m_\phi^2 - 4m_f^2))}{32\pi m_W^2 m_\phi^2}, \tag{2.39}$$

which leads to defining the theoretical Branching Ratio, as considered in section 2.1, which considers no pseudoscalar coupling $g_p = 0$,

$$\mathcal{B}^{theo}(\phi \rightarrow \bar{f}f) = \frac{\Gamma^{theo}_{\phi\rightarrow\bar{f}f}}{\Gamma^{theo}_{\phi,Tot}} = \frac{g_w^2 g_s^{(theo)2}(m_\phi^2 - 4m_f^2)^{\frac{3}{2}}}{32\pi m_W^2 m_\phi^2 \Gamma^{theo}_{\phi,Tot}}, \tag{2.40}$$

and taking the complete expression of the Partial Decay Width (equation 2.39), the expression for the observed Branching Ratio results:

$$\mathcal{B}^{obs}(\phi \rightarrow \bar{f}f) = \frac{\Gamma_{\phi\rightarrow\bar{f}f}}{\Gamma^{obs}_{\phi,Tot}} = \frac{g_w^2\sqrt{m_\phi^2 - 4m_f^2}(g_p^2 m_\phi^2 + g_s^2(m_\phi^2 - 4m_f^2))}{32\pi m_W^2 m_\phi^2 \Gamma^{obs}_{\phi,Tot}} \tag{2.41}$$

Ultimately, the Signal Strength of the $\phi\tau^+\tau^-$ interaction is built, considering the impact of the production and decay channels as well as the ratio of total widths $\frac{\Gamma^{obs}_{\phi,Tot}}{\Gamma^{theo}_{\phi,Tot}} \approx 1$:

$$\mu_{\tau\tau} = \frac{\mathcal{B}^{obs}(\phi \rightarrow \tau^+\tau^-)\sigma^{obs}(gg \rightarrow \phi)}{\mathcal{B}^{theo}(\phi \rightarrow \tau^+\tau^-)\sigma^{theo}(gg \rightarrow \phi)} = \frac{g_p^2 m_\phi^2 + g_s^2(m_\phi^2 - 4m_\tau^2)}{g_s^{(theo)2}(m_\phi^2 - 4m_\tau^2)}\kappa^2. \tag{2.42}$$

Conversely, the signal strength of the $\phi\bar{b}b$, as determined by equation 2.3, is:

$$\mu_{bb} = \frac{\mathcal{B}^{obs}(Z \to \phi Z)\mathcal{B}^{obs}(\phi \to \bar{b}b)}{\mathcal{B}^{theo}(Z \to \phi Z)\mathcal{B}^{theo}(\phi \to \bar{b}b)} = \frac{g_p^2 m_\phi^2 + g_s^2(m_\phi^2 - 4m_b^2)}{g_s^{(theo)2}(m_\phi^2 - 4m_b^2)}\kappa_z^2. \tag{2.43}$$

Here κ^2, as the ratio $\frac{\sigma^{obs}(gg\to\phi)}{\sigma^{theo}(gg\to\phi)}$ in the Signal Strength of the $\phi\gamma\gamma$ interaction, whereas $\kappa_z^2 = \frac{\mathcal{B}^{obs}(Z\to\phi Z)}{\mathcal{B}^{theo}(Z\to\phi Z)}$ in the $\phi\bar{b}b$ interaction; $m_\phi = 95.4$ GeV the ϕ boson mass, m_f the fermion mass, and $g_s^{(theo)} = \frac{m_f}{v}$ the Yukawa coupling in the SM. The next step is to graph values of g_s and g_p to find values that are within the limits established by ATLAS and CMS measurements in the $\phi \to \tau^+\tau^-$ and $\phi \to \bar{b}b$ channels (equations 2.7, 2.8).

Chapter 3

Analysis of Results

3.1 The $\phi \to \gamma\gamma$ decay.

In order to characterize this postulated new Higgs Boson (ϕ) with mass 95.4 GeV through the decays $\phi \to \gamma\gamma$, $\phi \to \tau^+\tau^-$, and $\phi \to \bar{b}b$, the characterization requires identifying permissible parameter values for $\mu_{\gamma\gamma}$, $\mu_{\tau\tau}$, and μ_{bb}, based on their experimentally reported Signal Strengths. For the $\phi\gamma\gamma$ interaction, the Signal Strength (equation 2.29) incorporates the $h_1^{\gamma\gamma}$ and $h_3^{\gamma\gamma}$ factors, which must be constrained to $0.16 \leq \mu_{\gamma\gamma} \leq 0.33$, as delineated by the limits specified in equation 2.6. These limits are multiplied by 1.96 to obtain results at a 95% Confidence Level, denoted statistically as 1.96σ. Consequently, the limits become:

$$0.0832 \leq \mu_{\gamma\gamma} \leq 0.4164. \tag{3.1}$$

Furthermore, incorporating the κ^2 term within the Signal Strength is beneficial for examining the influence of the production channel. The analysis considers three cases: initially, $\kappa = 1$; as a result, Beyond Standard Model (BSM) physics is excluded from the production channel. The second scenario utilizes $\kappa = \frac{1}{\sqrt{2}}$, indicating that the observed coupling is inferior to the theoretical prediction. Finally, the third case examines when $\kappa = \sqrt{2}$ is implemented to explain an excess in the observed channel.

3.1.1 Case 1: $\kappa^2 = 1$

Within the expression of the Signal Strength, the κ^2 factor appears, initially assumed as $\kappa^2 = 1$, indicating that the cross-sections $\sigma^{theo}(gg \to \phi)$ and $\sigma^{obs}(gg \to \phi)$ are equivalent. Firstly, it is imperative to determine the allowable values for the modules $h_1^{\gamma\gamma}$ and $h_3^{\gamma\gamma}$ (Figure 3.1). Given the context of modulus values for complex numbers, the presented data is inherently positive.

The figure 3.1 shows how the possible values of $|h_1^{\gamma\gamma}|$ and $|h_3^{\gamma\gamma}|$ are adjusted according to the limits imposed on the equation 3.1. Now, the tables 3.1 and 3.2 show possible numerical value ranges within the figure 3.1; the first table shows the lower and higher limits where we can find the values of $|h_1^{\gamma\gamma}|$ when we fix $|h_3^{\gamma\gamma}|$. The second table explores a proportional relationship $|h_1^{\gamma\gamma}| = \alpha|h_1^{\gamma\gamma}|$, varying α and showing how the allowed range for $|h_1^{\gamma\gamma}|$ changes accordingly, similar to how it was done in the table. 3.1. One observes that as the value of α grows, the allowed interval for $|h_1^{\gamma\gamma}|$ diminishes correspondingly.

Figure 3.2 presents four distinct scenarios where the parameter $h_3^{\gamma\gamma}$ within equation 2.29 is held constant. These scenarios are analyzed in conjunction with the constraints imposed by signal strength ($\mu_{\gamma\gamma}$), as reflected in the data presented in tables 3.1 and 3.2:

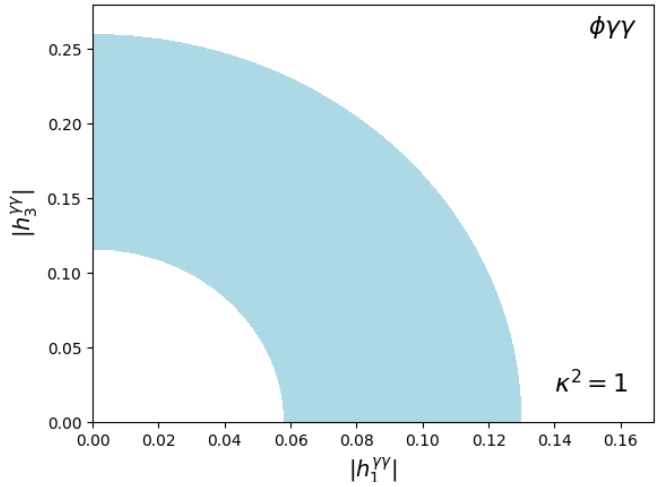

Figure 3.1: Permitted values for $|h_1^{\gamma\gamma}|$ and $|h_3^{\gamma\gamma}|$ with $\kappa^2 = 1$ in the $\phi \to \gamma\gamma$ decay

$\lvert h_3^{\gamma\gamma}\rvert$	$\lvert h_1^{\gamma\gamma}\rvert_{min}$	$\lvert h_1^{\gamma\gamma}\rvert_{max}$
0		0.129790
0.028842	0.056195	0.128986
0.057684	0.050339	0.126545
0.086527	0.038654	0.122367
0.116032	0	0.116102
0.144211	0	0.107918
0.187806	0	0.089597
0.201895	0	0.081578
0.230738	0	0.059460
0.259580	0	0

Table 3.1: Limits for $|h_1^{\gamma\gamma}|$ with $|h_3^{\gamma\gamma}|$ fixed and $\kappa^2 = 1$.

α	$\lvert h_1^{\gamma\gamma}\rvert_{min}$	$\lvert h_1^{\gamma\gamma}\rvert_{max}$
0.5	0.054698	0.122367
1.0	0.051891	0.116088
1.5	0.049476	0.110685
2.0	0.047370	0.105973
2.5	0.045511	0.101816
3.0	0.043856	0.098112
3.5	0.042369	0.094785
4.0	0.041023	0.091775
4.5	0.039799	0.089035
5.0	0.038677	0.086527

Table 3.2: Limits for $|h_1^{\gamma\gamma}|$ with $|h_3^{\gamma\gamma}| = \alpha|h_1^{\gamma\gamma}|$ and $\kappa^2 = 1$.

- **Scenario 1** postulates that $h_3^{\gamma\gamma}$ is zero; this means that there is no CP-violation. $|h_1^{\gamma\gamma}|$ has values restricted to $|h_1^{\gamma\gamma}| \in [0.058016, 0.129790]$.
- **Scenario 2** examines $|h_3^{\gamma\gamma}|$ at its minimal permissible value where $|h_1^{\gamma\gamma}|$ can be zero, specifically $|h_3^{\gamma\gamma}| = 0.116032$. This scenario permits values for $|h_1^{\gamma\gamma}| \in [0, 0.116102]$. However, at the maximal permitted value of $|h_3^{\gamma\gamma}|$, no values remain within the signal strength constraints.
- **Scenario 3** graphs the permissible values for $|h_3^{\gamma\gamma}| = 2|h_1^{\gamma\gamma}|$, where it is noted that the allowable range becomes constricted to $|h_1^{\gamma\gamma}| \in [0.047370, 0.105973]$, as detailed in table 3.2.
- The final scenario, **scenario 4**, adopts the midpoint between $|h_3^{\gamma\gamma}|_{min} = 0.116032$ and $|h_3^{\gamma\gamma}|_{max} = 0.259580$, the lower and upper limits when $|h_1^{\gamma\gamma}| = 0$; thus, $|h_3^{\gamma\gamma}|_{mid} = 0.187806$ allows a range of $|h_1^{\gamma\gamma}| \in [0, 0.089597]$.

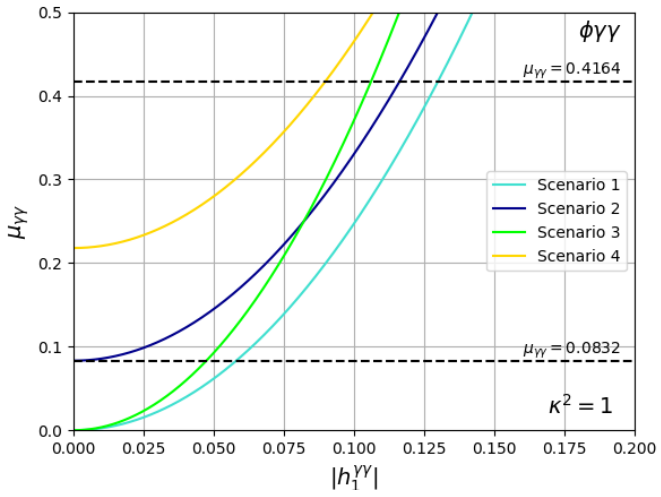

Figure 3.2: Permitted values for $|h_1^{\gamma\gamma}|$ with $|h_3^{\gamma\gamma}|$ fixed and $\kappa^2 = 1$ in the $\phi \to \gamma\gamma$ decay

Up to now, these analyses have utilized the modules of $h_1^{\gamma\gamma}$ and $h_3^{\gamma\gamma}$. However, these are complex quantities necessitating the analysis of their real and imaginary components:

- Figure 3.3a shows a ring zone area, the permitted domain of $h_1^{\gamma\gamma}$ raised in **scenario 1** where the CP symmetry is conserved.
- The graph on figure 3.3b is closed at the origin; this is the **scenario 2** where $|h_3^{\gamma\gamma}|$ takes the minimum value at which $|h_1^{\gamma\gamma}|$ can be zero.
- In figure 3.3c the domain returns to form a notable ring region; here the domain is described according to the **scenario 3** that conditions a direct relation with the magnitude of the CP-violating term.
- Ultimately, figure 3.3d corresponds to a circular domain of $h_1^{\gamma\gamma}$ in the **scenario 4**, which reflects an intermediate constraint on the magnitude of the CP-conserving term in the moderate presence of the CP-violating term.

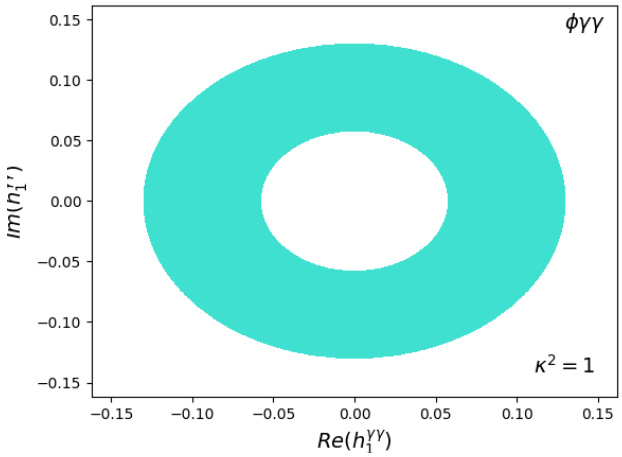

(a) Domain of $h_1^{\gamma\gamma}$ with $|h_3^{\gamma\gamma}| = 0$ with $\kappa^2 =$ in the $\phi \to \gamma\gamma$ decay

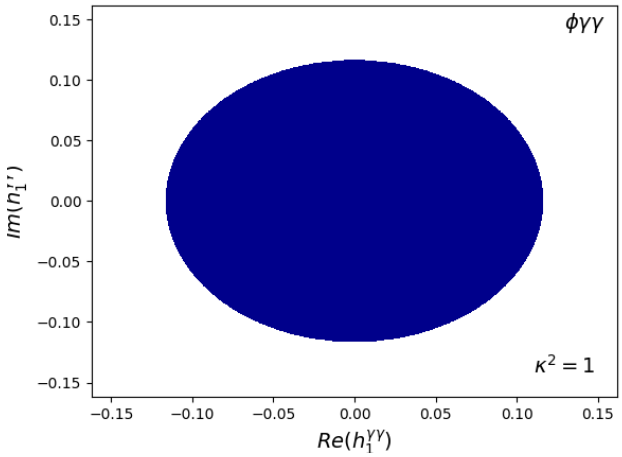

(b) Domain of $h_1^{\gamma\gamma}$ with $|h_3^{\gamma\gamma}| = |h_3^{\gamma\gamma}|_{min}$ with $\kappa^2 = 1$ in the $\phi \to \gamma\gamma$ decay

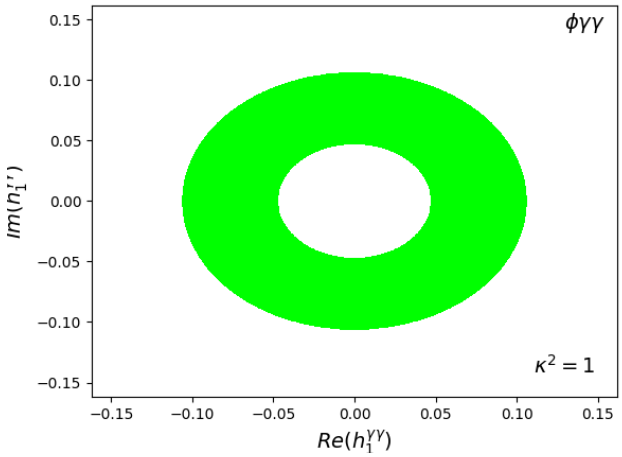

(c) Domain of $h_1^{\gamma\gamma}$ with $|h_3^{\gamma\gamma}| = 2|h_3^{\gamma\gamma}|$ with $\kappa^2 = 1$ in the $\phi \to \gamma\gamma$ decay

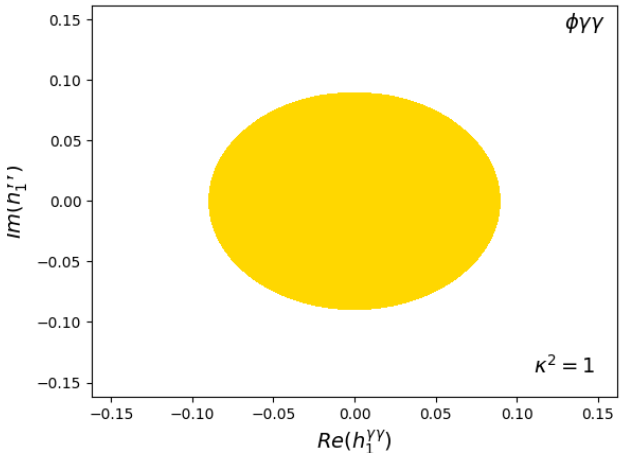

(d) Domain of $h_1^{\gamma\gamma}$ with $|h_3^{\gamma\gamma}| = |h_3^{\gamma\gamma}|_{mid}$ with $\kappa^2 = 1$ in the $\phi \to \gamma\gamma$ decay

Figure 3.3: Domain of $h_1^{\gamma\gamma}$ for each scenario in figure 3.2

3.1.2 Case 2: $\kappa^2 = 0.5$

The second scenario considers $\kappa = \frac{1}{\sqrt{2}}$. This case is analyzed following the same approach outlined previously in subsection 3.1.1, ensuring consistency and comparability of results. The figure 3.4 shows the permissible values of the modules of $h_1^{\gamma\gamma}$ and $h_3^{\gamma\gamma}$. Similar to the preceding scenario, the magnitudes displayed remain strictly positive.

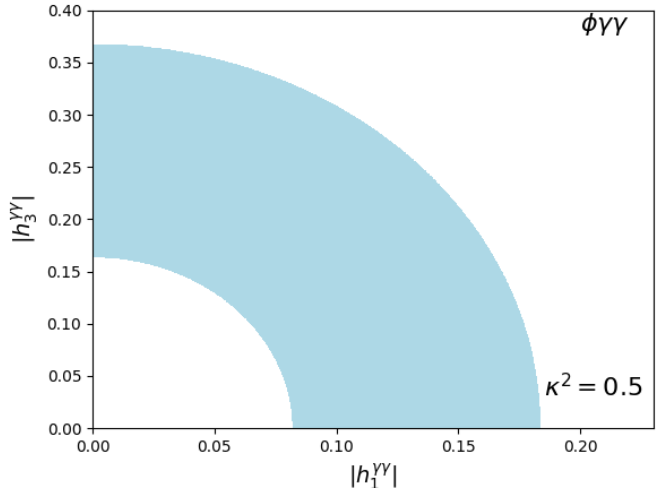

Figure 3.4: Permitted values for $|h_1^{\gamma\gamma}|$ and $|h_3^{\gamma\gamma}|$ with $\kappa^2 = 0.5$ in the $\phi \to \gamma\gamma$ decay

From the figure 3.4, the table 3.3 fixes $|h_3^{\gamma\gamma}|$; while in table 3.4 the relationship between the two form factors is explicitly set as $|h_3^{\gamma\gamma}| = \alpha|h_1^{\gamma\gamma}|$, varying the parameter α. Both tables give the minimum and maximum limits of $|h_1^{\gamma\gamma}|$.

$\lvert h_3^{\gamma\gamma}\rvert$	$\lvert h_1^{\gamma\gamma}\rvert_{min}$	$\lvert h_1^{\gamma\gamma}\rvert_{max}$
0	0.082047	0.183551
0.040789	0.079472	0.182414
0.081578	0.071190	0.178961
0.122367	0.054665	0.173053
0.164094	0	0.164192
0.203945	0	0.152619
0.244734	0	0.136811
0.265598	0	0.126709
0.326312	0	0.084089
0.367101	0	0

Table 3.3: Limits for $|h_1^{\gamma\gamma}|$ with $|h_3^{\gamma\gamma}|$ fixed and $\kappa^2 = 0.5$.

α	$\lvert h_1^{\gamma\gamma}\rvert_{min}$	$\lvert h_1^{\gamma\gamma}\rvert_{max}$
0.5	0.077355	0.173053
1.0	0.073385	0.164173
1.5	0.069970	0.156533
2.0	0.066991	0.149868
2.5	0.064363	0.143989
3.0	0.062022	0.138751
3.5	0.059919	0.134046
4.0	0.058016	0.129790
4.5	0.056284	0.125915
5.0	0.054698	0.122367

Table 3.4: Limits for $|h_1^{\gamma\gamma}|$ with $|h_3^{\gamma\gamma}| = \alpha|h_1^{\gamma\gamma}|$ and $\kappa^2 = 0.5$.

The four scenarios described previously are revisited in figure 3.5, highlighting how their allowed regions differ from those in the first case:

- **Scenario 1** takes $|h_3^{\gamma\gamma}| = 0$, which leaves $|h_1^{\gamma\gamma}|$ constrained to $|h_1^{\gamma\gamma}| \in [0.082047, 0.183551]$.
- The **scenario 2** takes $|h_3^{\gamma\gamma}| = 0.164094$, which is the minimum value of $|h_3^{\gamma\gamma}|$ where $|h_1^{\gamma\gamma}|$ can be zero, this leads to $|h_1^{\gamma\gamma}| \in [0, 0.164192]$.
- **Scenario 3** restricts $|h_1^{\gamma\gamma}|$ to the range $0.066991 \leq |h_1^{\gamma\gamma}| \leq 0.149868$ under the condition $|h_3^{\gamma\gamma}| = 2|h_1^{\gamma\gamma}|$.
- Finally, the **scenario 4** takes the middle value of $|h_3^{\gamma\gamma}| = 0.265598$ to analyze an intermediate influence of the CP-violating term. $|h_1^{\gamma\gamma}|$ is constrained to $|h_1^{\gamma\gamma}| \in [0, 0.126709]$.

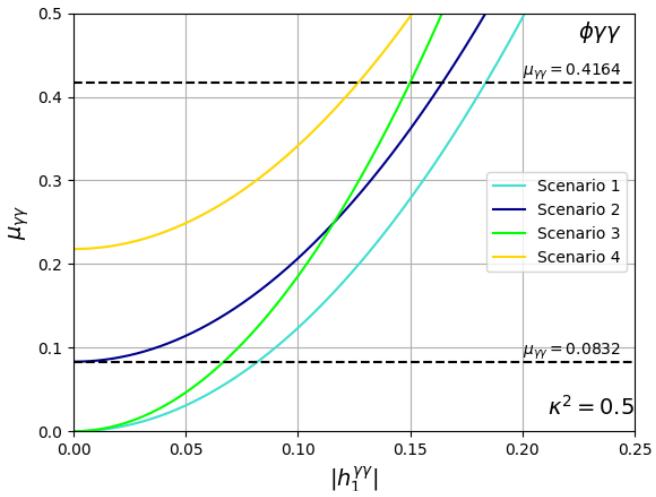

Figure 3.5: Permitted values for $|h_1^{\gamma\gamma}|$ with $|h_3^{\gamma\gamma}|$ fixed and $\kappa^2 = 0.5$ in the $\phi \to \gamma\gamma$ decay

From these scenarios, the real and imaginary components of $h_1^{\gamma\gamma}$ are explored:

- Figure 3.6a shows the domain of $h_1^{\gamma\gamma}$ in the **scenario 1**, which does not consider the CP-violating factor, and according to figure 3.4, $|h_1^{\gamma\gamma}|$ cannot be zero when $|h_3^{\gamma\gamma}| = 0$, thus the domain is in a ring region.
- The **scenario 2** describes the Signal Strength through $|h_3^{\gamma\gamma}| = o : 0.164094$, which is the minimal value of $|h_3^{\gamma\gamma}|$ where $|h_1^{\gamma\gamma}|$ can be zero, so the domain of $h_1^{\gamma\gamma}$ in figure 3.6b is given by a closed circular area.
- When $|h_3^{\gamma\gamma}| = 2|h_1^{\gamma\gamma}|$ in the **scenario 3**, the domain returns to a ring shape because $|h_1^{\gamma\gamma}|$ cannot be zero, or the expression of the Signal Strength (equation 2.29) would be zero, which is out of bounds of the equation 3.1.
- Figure 3.6d related to **scenario 4** represents the domain of $h_1^{\gamma\gamma}$ considering an intermediate CP-violating influence, selecting the midpoint $|h_3^{\gamma\gamma}|_{mid} = 0.265598$. Observe that the region in figure 3.6b is smaller than in figure 3.6b, reflecting the tighter constraints imposed by larger values of $|h_3^{\gamma\gamma}|$ (see table 3.3).

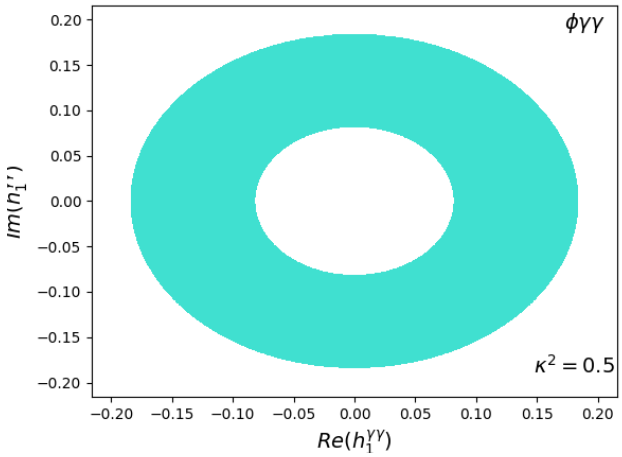

(a) Domain of $h_1^{\gamma\gamma}$ with $|h_3^{\gamma\gamma}| = 0$ with $\kappa^2 = 0.5$ in the $\phi \to \gamma\gamma$ decay

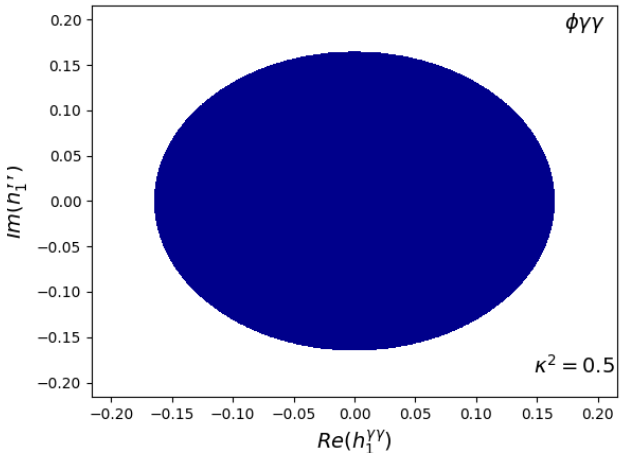

(b) Domain of $h_1^{\gamma\gamma}$ with $|h_3^{\gamma\gamma}| = |h_3^{\gamma\gamma}|_{min}$ with $\kappa^2 = 0.5$ in the $\phi \to \gamma\gamma$ decay

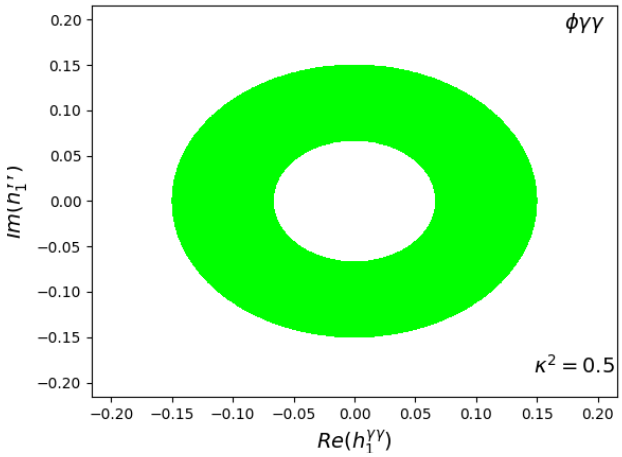

(c) Domain of $h_1^{\gamma\gamma}$ with $|h_3^{\gamma\gamma}| = 2|h_3^{\gamma\gamma}|$ with $\kappa^2 = 0.5$ in the $\phi \to \gamma\gamma$ decay

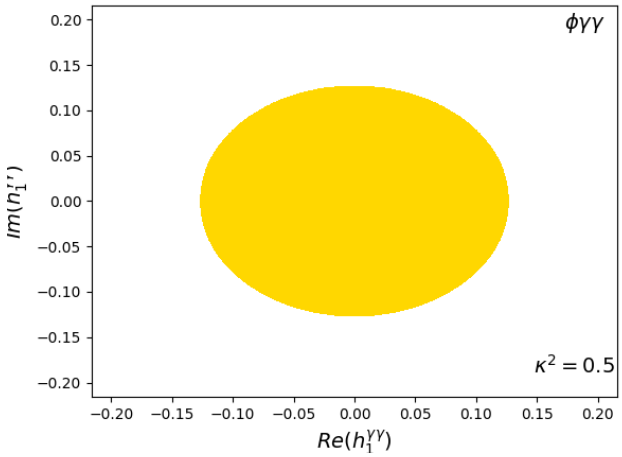

(d) Domain of $h_1^{\gamma\gamma}$ with $|h_3^{\gamma\gamma}| = |h_3^{\gamma\gamma}|_{mid}$ with $\kappa^2 = 0.5$ in the $\phi \to \gamma\gamma$ decay

Figure 3.6: Domain of $h_1^{\gamma\gamma}$ for each scenario in figure 3.5

3.1.3 Case 3: $\kappa^2 = 2$

Case 3 examines the scenario that serves as a counterpart to the second case, where $\kappa = \sqrt{2}$ is noted as an excess of the observed Cross-Section. Figure 3.7 illustrates a more constrained region of permissible values for $|h_1^{\gamma\gamma}|$ and $|h_3^{\gamma\gamma}|$ relative to preceding cases, with all values being strictly positive.

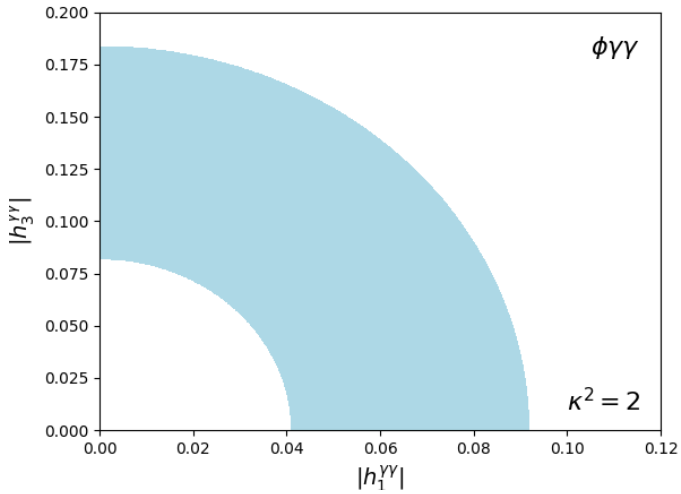

Figure 3.7: Permitted values for $|h_1^{\gamma\gamma}|$ and $|h_3^{\gamma\gamma}|$ with $\kappa^2 = 2$ in the $\phi \to \gamma\gamma$ decay

Here the table 3.5 contains the minimum and maximum values of $|h_1^{\gamma\gamma}|$ with $|h_3^{\gamma\gamma}|$ fixed. The values shown in this case are significantly smaller by about an order of magnitude compared to the results from earlier cases (Tables 3.3 and 3.1). A similar situation occurs with the table 3.6, which takes the situation of $|h_3^{\gamma\gamma}| = \alpha|h_1^{\gamma\gamma}|$, emphasizing that as the proportionality factor α increases, the range of permitted values of $|h_1^{\gamma\gamma}|$ consistently becomes narrower.

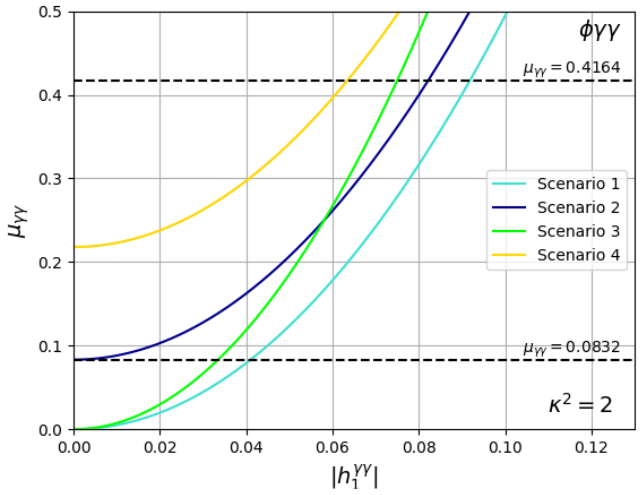

Figure 3.8: Permitted values for $|h_1^{\gamma\gamma}|$ with $|h_3^{\gamma\gamma}|$ fixed and $\kappa^2 = 2$ in the $\phi \to \gamma\gamma$ decay

$\lvert h_3^{\gamma\gamma}\rvert$	$\lvert h_1^{\gamma\gamma}\rvert_{min}$	$\lvert h_1^{\gamma\gamma}\rvert_{max}$
0	0.041023	0.091775
0.020395	0.039736	0.091207
0.040789	0.035595	0.089481
0.061184	0.027333	0.086527
0.082047	0.004379	0.082096
0.101973	0	0.076309
0.122367	0	0.068405
0.132799	0	0.063355
0.163156	0	0.042044
0.183551	0	0

Table 3.5: Limits for $\lvert h_1^{\gamma\gamma}\rvert$ with $\lvert h_3^{\gamma\gamma}\rvert$ fixed and $\kappa^2 = 2$.

α	$\lvert h_1^{\gamma\gamma}\rvert_{min}$	$\lvert h_1^{\gamma\gamma}\rvert_{max}$
0.5	0.038677	0.086527
1.0	0.036692	0.082086
1.5	0.034985	0.078266
2.0	0.033496	0.074934
2.5	0.032181	0.071994
3.0	0.031011	0.069376
3.5	0.029959	0.067023
4.0	0.029008	0.064895
4.5	0.028142	0.062957
5.0	0.027349	0.061184

Table 3.6: Limits for $\lvert h_1^{\gamma\gamma}\rvert$ with $\lvert h_3^{\gamma\gamma}\rvert = \alpha\lvert h_1^{\gamma\gamma}\rvert$ and $\kappa^2 = 2$.

Figure 3.8 plots $\mu_{\gamma\gamma}$ according to four scenarios already discussed in the previous cases:

- The **scenario 1** does not consider the CP-violating factor, thus $\lvert h_3^{\gamma\gamma}\rvert = 0$, which yields a range of $\lvert h_1^{\gamma\gamma}\rvert \in [0.041023, 0.091775]$.
- **Scenario 2** takes $\lvert h_3^{\gamma\gamma}\rvert = 0.082047$ being this the minimum value of $\lvert h_3^{\gamma\gamma}\rvert$ where $\lvert h_1^{\gamma\gamma}\rvert$ can be zero; therefore, $\lvert h_1^{\gamma\gamma}\rvert \in [0, 0.082096]$.
- **Scenario 3** constrains $0.033496 \leq \lvert h_1^{\gamma\gamma}\rvert \leq 0.074934$, in the situation of $\lvert h_3^{\gamma\gamma}\rvert = 2\lvert h_1^{\gamma\gamma}\rvert$.
- $\lvert h_3^{\gamma\gamma}\rvert = 0.132799$ is the middle value that $\lvert h_3^{\gamma\gamma}\rvert$ can take where $\lvert h_1^{\gamma\gamma}\rvert$ can be zero, this represents the **scenario 4** and takes into account an intermediate influence of the CP-violating term, leaving a range of $\lvert h_1^{\gamma\gamma}\rvert \in [0, 0.063355]$.

Analyzing the domain of $h_1^{\gamma\gamma}$ in the **scenario 1**, the ring zone shown in figure 3.9a is similar to those in figures 3.6a and 3.3a, with a notably smaller domain, a direct consequence of the increased value of κ. A similar situation occurs in the closed circle of the **scenario 2**, where $\lvert h_1^{\gamma\gamma}\rvert$ can be zero, resulting in a further constriction of the $h_1^{\gamma\gamma}$ domain. Figure 3.9c continues showing a ring area, but as with scenarios 1 and 2, its area is more restricted. Finally, the figure 3.9d shows an even more restricted circular area due to a greater influence of $\lvert h_3^{\gamma\gamma}\rvert$, in addition to the restrictive effect introduced by the value $\kappa^2 = 2$.

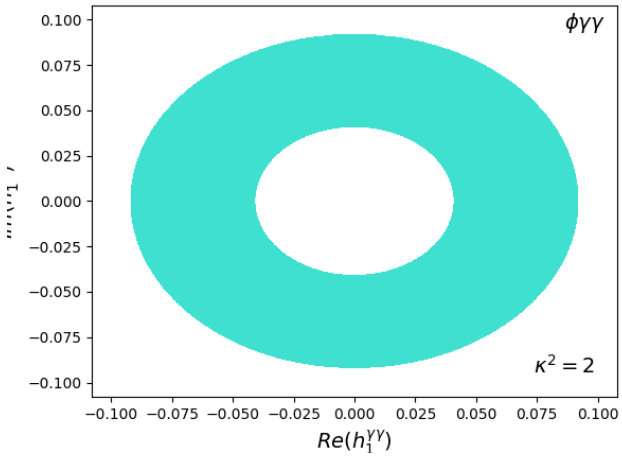

(a) Domain of $h_1^{\gamma\gamma}$ with $|h_3^{\gamma\gamma}| = 0$ with $\kappa^2 = 2$ in the $\phi \to \gamma\gamma$ decay

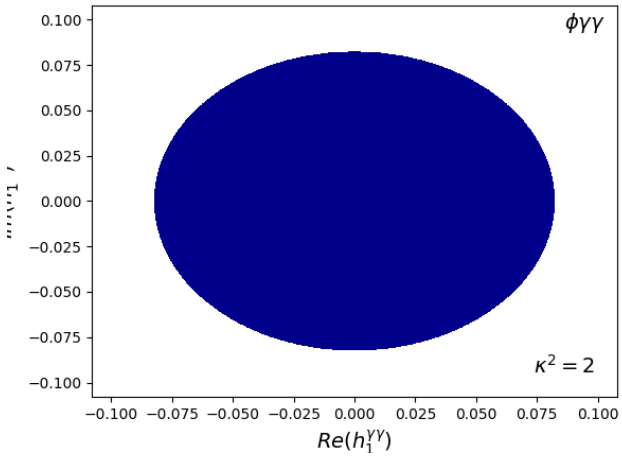

(b) Domain of $h_1^{\gamma\gamma}$ with $|h_3^{\gamma\gamma}| = |h_3^{\gamma\gamma}|_{min}$ with $\kappa^2 = 2$ in the $\phi \to \gamma\gamma$ decay

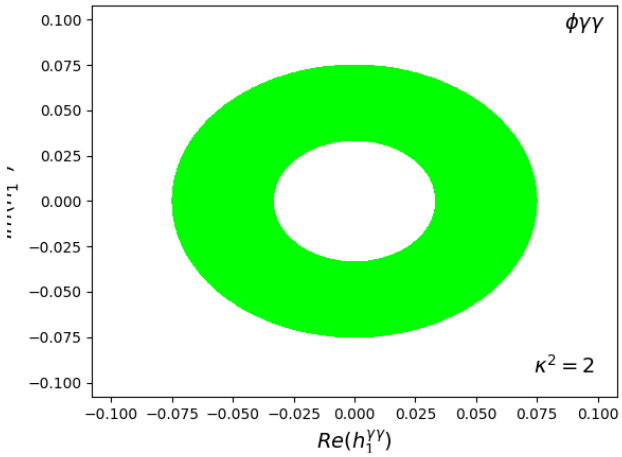

(c) Domain of $h_1^{\gamma\gamma}$ with $|h_3^{\gamma\gamma}| = 2|h_3^{\gamma\gamma}|$ with $\kappa^2 = 2$ in the $\phi \to \gamma\gamma$ decay

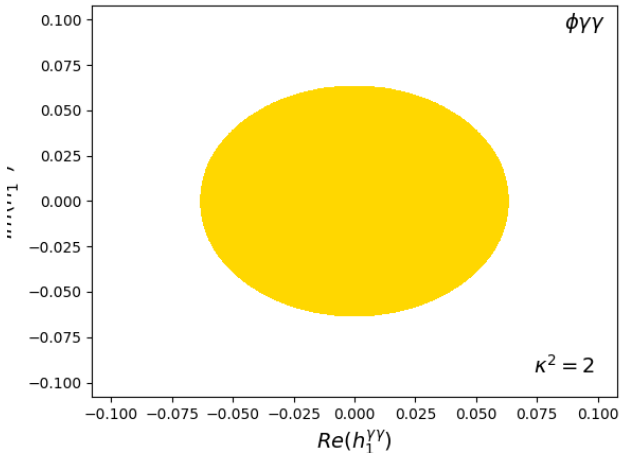

(d) Domain of $h_1^{\gamma\gamma}$ with $|h_3^{\gamma\gamma}| = |h_3^{\gamma\gamma}|_{mid}$ with $\kappa^2 = 2$ in the $\phi \to \gamma\gamma$ decay

Figure 3.9: Domain of $h_1^{\gamma\gamma}$ for each scenario in figure 3.8

3.2 The $\phi \to \tau^+\tau^-$ decay.

The decay $\phi \to \tau^+\tau^-$ is studied by constraining its Signal Strength (equation 2.43) with experimental observations (equation 2.7). Thus, the scalar and pseudoscalar couplings, g_s^τ and g_p^τ respectively, from the expression 2.43 must fulfill $0.7 \leq \mu_{\tau\tau} \leq 1.7$, but considering a 95% of Confidence Level, this range is adjusted to:

$$0.22 \leq \mu_{\tau\tau} \leq 2.18. \tag{3.2}$$

The κ^2 term is used to model how the ratio between observed and theoretical production cross-sections affects the behavior of the expression for the Signal Strength for fermions (equation 2.43). The fermion mass $m_f = m_\tau = 1.7769$ GeV is taken, and three different cases for κ^2 values: $\sigma^{obs}(gg \to \phi) = \sigma^{theo}(gg \to \phi)$ for $\kappa^2 = 1$, $\sigma^{obs}(gg \to \phi) = \frac{1}{2}\sigma^{theo}(gg \to \phi)$ for $\kappa^2 = 0.5$, and $\sigma^{obs}(gg \to \phi) = 2\sigma^{theo}(gg \to \phi)$ for $\kappa^2 = 2$.

3.2.1 Case 1: $\kappa^2 = 1$

Figure 3.10 shows that the region of permitted values for g_s^τ and g_p^τ is an almost completely circular ring area, in contrast with the graphs of the $\phi\gamma\gamma$ interaction, which only showed the first quadrant. In contrast to the previous analysis, here g_s^τ and g_p^τ are real parameters and can take both positive and negative values. In particular, values arbitrarily close to zero are not allowed, which restricts that only one of the values between g_s^τ and g_p^τ can be zero.

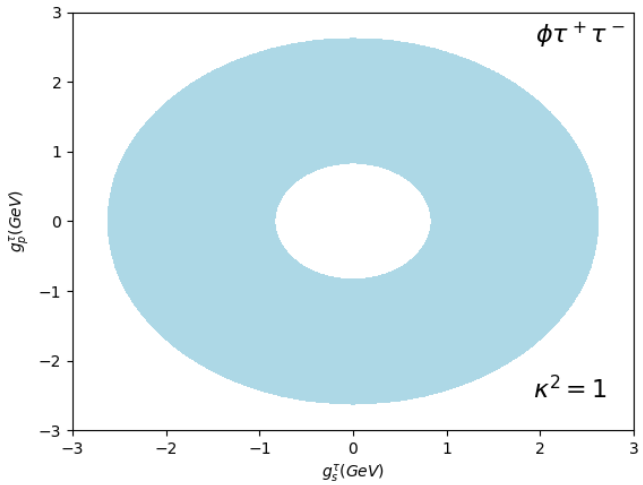

Figure 3.10: Permitted values for g_s^τ and g_p^τ with $\kappa^2 = 1$ in the $\phi \to \tau^+\tau^-$ decay.

Table 3.7 fixes g_p^τ and presents the minimum and maximum values that g_s^τ can take. However, since there is an inner circle of non-allowed values, values in the table of $g_{s,min}^\tau$ and $g_{s,max}^\tau$ from $g_p^\tau = -0.524348$ GeV to $g_p^\tau = 0.524348$ GeV can be switched if their negatives are taken. Note that when $g_s^\tau = 0$ GeV in the last row, the maximum value of g_p^τ is 2.621740 GeV; while in the middle row, when $g_p^\tau = 0$ GeV, $g_{s,max}^\tau = 2.623561$ GeV. This indicates that, although figure 3.10 shows an apparently circular ring, it is actually a very slightly flattened oval along the g_p^τ-axis.

A different situation is when $g_p^\tau \propto g_s^\tau$ is taken. The proportionality factor α is given in table 3.8 and shows how, as α becomes higher, the range between $g_{s,min}^\tau$ and $g_{s,max}^\tau$ becomes narrower, in the same way as it did in the $\phi\gamma\gamma$ interaction.

The behavior of the Signal Strength ($\mu_{\tau\tau}$) in function of g_s^τ is detailed in figure 3.11. Four different scenarios for g_p^τ are planned:

g_p^τ (GeV)	$g_{s,min}^\tau$ (GeV)	$g_{s,max}^\tau$ (GeV)
-2.621740	0	0
-2.097392	-1.574137	1.574137
-1.573044	-2.098849	2.098849
-1.048696	-2.404534	2.404534
-0.524348	0.647533	2.570555
0	0.833440	2.623561
0.524348	0.647533	2.570555
0.832862	-2.487660	2.487660
1.727301	-1.973667	1.973667
2.097392	-1.574137	1.574137
2.621740	0	0

Table 3.7: Limits for g_s^τ with g_p^τ fixed and $\kappa^2 = 1$.

α	$g_{s,min}^\tau$ (GeV)	$g_{s,max}^\tau$ (GeV)
0.5	0.680343	2.141633
1.0	0.589126	1.854494
1.5	0.526894	1.658595
2.0	0.480964	1.514013
2.5	0.445271	1.401657
3.0	0.416503	1.311098
3.5	0.392675	1.236091
4.0	0.372519	1.172641
4.5	0.355178	1.118055
5.0	0.340054	1.070445
5.5	0.326710	1.028441

Table 3.8: Limits for g_s^τ with $g_p^\tau = \alpha g_s^\tau$ and $\kappa^2 = 1$.

- **Scenario 1** considers no CP-violation $g_p^\tau = 0$ GeV. This scenario has a parabola symmetrically cut in the middle, since it does not consider the CP-violating term; as shown in figure 3.10, its domain crosses the central zone of disallowed values, this is $g_s^\tau \in [-3.710276, -1.178662] \cup [1.178662, 3.710276]$.
- **Scenario 2** describes $\mu_{\tau\tau}$ taken $g_p^\tau = 0.832862$ GeV, which are the values in the limit of the inner circle where g_s^τ can be zero. In this scenario, there is a continuous parabola inside of the limits for permitted values of g_s^τ, which yields to $g_s^\tau \in [-2.487660, 2.487660]$.
- **Scenario 3** takes the proportionality term $\alpha = 2$ as done in the development of table 3.8. The g_s^τ domain is $g_s^\tau \in [-1.514013, -0.480964] \cup [0.480964, 1.514013]$, maintaining the restriction that neither g_s^τ nor g_p^τ can be zero simultaneously.
- Finally, **scenario 4** considers an intermediate CP-violating scenario, selecting the midpoint $g_{p,mid}^\tau = 1.727301$ GeV between the values $g_{p,min}^\tau = 0.832862$ GeV and $g_{p,max}^\tau = 2.621740$ GeV where g_s^τ can be zero. The difference with scenario 2 is that there is more influence of the CP-violating factor g_p^τ, which reduces the domain to $g_s^\tau \in [-1.973667, 1.973667]$. The latter scenario is equivalent to taking $g_{s,mid}^\tau = -1.727301$ GeV, which is the middle value between $g_{p,min}^\tau = -2.621740$ GeV and $g_{p,max}^\tau = -0.832862$ GeV, due to there being only one quadratic term of g_s^τ in the expression of the Signal Strength (equation 2.43).

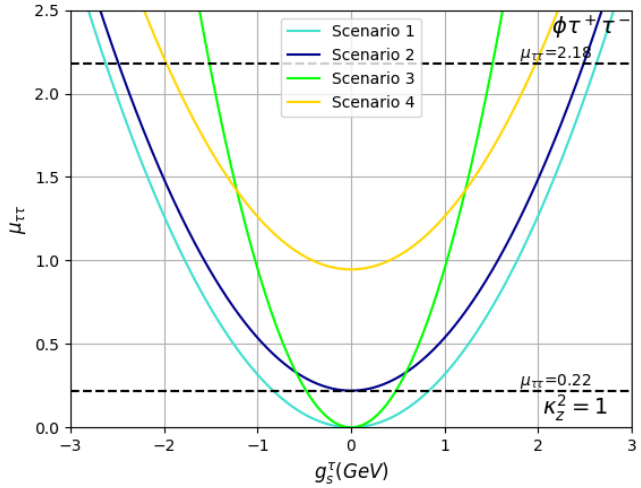

Figure 3.11: Permitted values for g_s^τ with g_p^τ fixed and $\kappa^2 = 1$ in the $\phi \to \tau^+\tau^-$ decay.

3.2.2 Case 2: $\kappa^2 = 0.5$

The relation $\sigma^{obs}(gg \to \phi) = \frac{1}{2}\sigma^{theo}(gg \to \phi)$ is taken to leave $\kappa^2 = 0.5$. Compared to figure 3.12, figure 3.10 shows a larger region of permissible values, due to the reduced effect of κ^2.

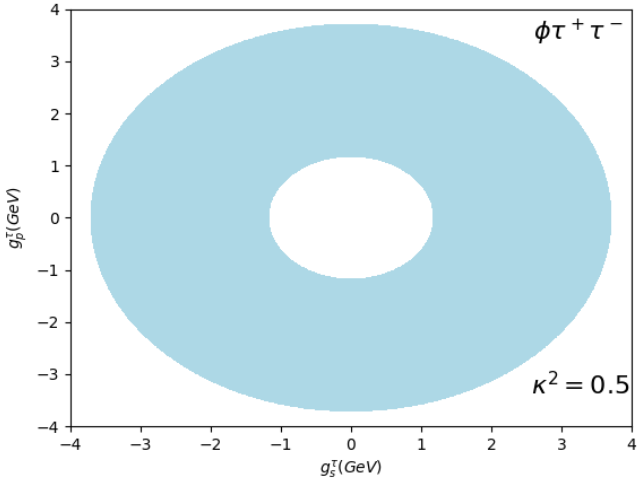

Figure 3.12: Permitted values for g_s^τ and g_p^τ with $\kappa^2 = 0.5$ in the $\phi \to \tau^+\tau^-$ decay.

Table 3.9 is constructed by fixing g_p^τ at equally spaced intervals from its lowest to its highest value. Note that the maximum value of g_s^τ when $g_p^\tau = 0$ GeV is greater than the maximum value of g_p^τ, showing that the region of permitted values is not a perfect circular ring. Table 3.10 considers g_s^τ proportional to g_p^τ through the α factor ($g_p^\tau = \alpha g_s^\tau$); and gives the minimum and maximum values that g_s^τ can take. The same pattern as in the previous case is observed in that, as α increases, the range of permissible values of g_s^τ decreases.

The four scenarios discussed in the previous case are considered to build figure 3.13, in which it is noted that:

g_p^τ (GeV)	$g_{s,min}^\tau$ (GeV)	$g_{s,max}^\tau$ (GeV)
-3.707701	0	0
-2.966161	-2.226166	2.226166
-2.224621	-2.968221	2.968221
-1.483080	-3.400524	3.400524
-0.741540	0.915750	3.635313
0	1.178662	3.710276
0.741540	0.915750	3.635313
1.177844	-3.518083	3.518083
2.442772	-2.791186	2.791186
2.966161	-2.226166	2.226166
3.707701	0	0

Table 3.9: Limits for g_s^τ with g_p^τ fixed and $\kappa^2 = 0.5$.

α	$g_{s,min}^\tau$ (GeV)	$g_{s,max}^\tau$ (GeV)
0.5	0.962151	3.028726
1.0	0.833151	2.622650
1.5	0.745141	2.345607
2.0	0.680186	2.141137
2.5	0.629709	1.982242
3.0	0.589024	1.854172
3.5	0.555327	1.748097
4.0	0.526821	1.658364
4.5	0.502298	1.581168
5.0	0.480908	1.513838
5.5	0.462038	1.454435

Table 3.10: Limits for g_s^τ with $g_p^\tau = \alpha g_s^\tau$ and $\kappa^2 = 0.5$.

- **Scenario 1**, which neglects the CP-violating term g_p^τ, exhibits a parabola cut symmetrically on the g_s^τ-axis, thereby partitioning the domain of g_s^τ into its positive and negative values: $g_s^\tau \in [-3.710276, -1.178662] \cup [1.178662, 3.710276]$.
- **Scenario 2** presents a continuous parabola, with a sufficiently significant influence of $g_p^\tau = 1.177844$ GeV to permit $g_s^\tau = 0$ GeV; should this value represent the maximum permissible of g_p^τ, only a singular potential value for g_s^τ remains: $g_s^\tau = 0$ GeV. The domain remains unsegmented $g_s^\tau \in [-3.518083, 3.518083]$.
- In the **scenario 3**, wherein $g_p^\tau = 2g_s^\tau$ is considered, has the same detail as scenario 1, since g_s^τ exclusively affects the Signal Strength mathematically, leading the domain to yield $g_s^\tau \in [-2.141137, -0.680186] \cup [0.680186, 2.141137]$.
- **Scenario 4**, as in scenario 2, presents a continuous parabola, being unique scenarios explored where the value of $g_s^\tau = 0$ GeV is admissible; however, differing in the size of the domain of g_s^τ due to the increased effect of g_p^τ, resulting in fewer values: $g_p^\tau = 2.442772 GeV \Rightarrow g_s^\tau \in [-2.791186, 2.791186]$.

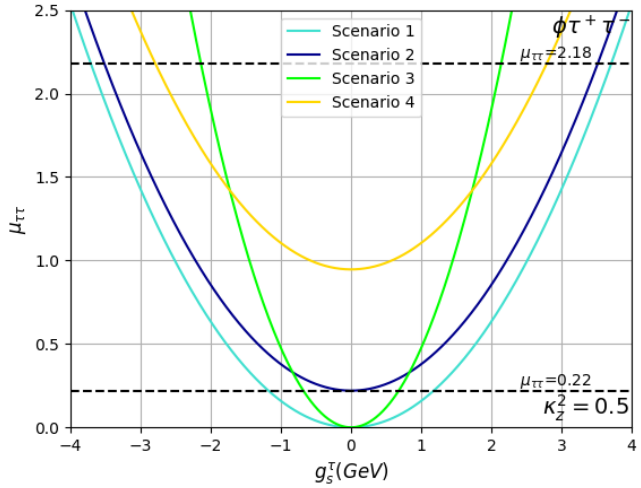

Figure 3.13: Permitted values for g_s^τ with g_p^τ fixed and $\kappa^2 = 0.5$ in the $\phi \to \tau^+\tau^-$ decay.

3.2.3 Case 3: $\kappa^2 = 2$

The last case considers $\sigma^{obs}(gg \to \phi) = 2\sigma^{theo}(gg \to \phi) \to \kappa^2 = 2$. A stronger effect of κ implies a stronger constraint on the g_s^τ and g_p^τ domains. This is visible in figure 3.14, whose limits are much more restricted than those shown in figure 3.12, with a smaller effect of κ.

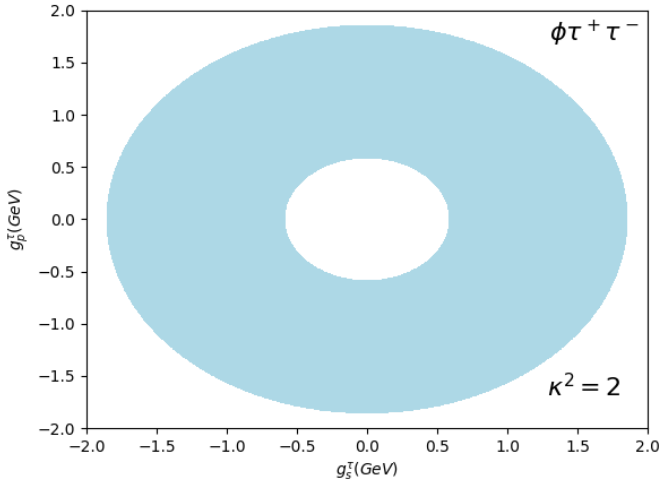

Figure 3.14: Permitted values for g_s^τ and g_p^τ with $\kappa^2 = 2$

The tables 3.11 and 3.12 show data for g_p^τ fixed and $g_s^\tau \propto g_s^\tau$ respectively. It is evident from the first table that the maximum allowed g_s^τ differs slightly depending on whether $g_p^\tau = 0$ GeV is zero or takes its maximal permissible value. Note that, as in the previous cases, values in the table from $g_p^\tau = -0.370770$ GeV to $g_p^\tau = 0.370770$ GeV switch when their negative is taken; this considers the area inside the ring of non-permitted values in figure 3.14. The second one takes α as the proportionality factor of $g_p^\tau \propto g_s^\tau$, repeating the pattern of $\alpha \to \infty \Rightarrow g_{s,min}^\tau \simeq g_{s,max}^\tau$, reducing the domain of g_s^τ.

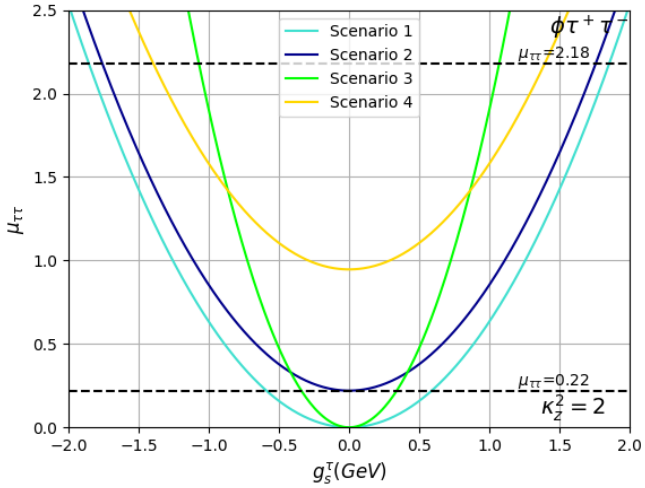

Figure 3.15: Permitted values for g_s^τ with g_p^τ fixed and $\kappa^2 = 2$ in the $\phi \to \tau^+\tau^-$ decay.

Figure 3.15 shows the behavior of the Signal Strength in terms of g_s^τ, under the same previously explored four scenarios:

- **Scenario 1** exhibits a symmetric domain around the origin, spanning two intervals: from $g_{s,min}^\tau = -1.855138$ GeV to $g_{s,max}^\tau = -0.589331$ GeV and from $g_{s,min}^\tau = 0.589331$ GeV to $g_{s,max}^\tau = 1.855138$ GeV.
- **Scenario 2** considers the influence of g_p^τ sufficiently large so that g_s^τ can be zero; this allows the domain of the parabola to be continuous: $g_p^\tau = 0.588922 GeV \Rightarrow g_s^\tau \in [-1.759041, 1.759041]$.
- The **scenario 3** shows a narrower parabola than in scenario 1, but it is also cut symmetrically in the middle, having a domain from g_s^τ-axis that yields $g_s^\tau \in [-1.070569, -0.340093] \cup [0.340093, 1.070569]$.
- Finally, **scenario 4** shows a continuous parabola with fewer permitted values than those in scenario 2, due to a greater influence of g_p^τ: $g_{p,mid}^\tau = 1.221386 GeV \Rightarrow g_s^\tau \in [-1.395593, 1.395593]$.

g_p^τ (GeV)	$g_{s,min}^\tau$ (GeV)	$g_{s,max}^\tau$ (GeV)
-1.853850	0	0
-1.483080	-1.113083	1.113083
-1.112310	-1.484110	1.484110
-0.741540	-1.700262	1.700262
-0.370770	0.457875	1.817657
0	0.589331	1.855138
0.370770	0.457875	1.817657
0.588922	-1.759041	1.759041
1.221386	-1.395593	1.395593
1.483080	-1.113083	1.113083
1.853850	0	0

Table 3.11: Limits for g_s^τ with g_p^τ fixed and $\kappa^2 = 2$.

α	$g_{s,min}^\tau$ (GeV)	$g_{s,max}^\tau$ (GeV)
0.5	0.481075	1.514363
1.0	0.416575	1.311325
1.5	0.372570	1.172804
2.0	0.340093	1.070569
2.5	0.314854	0.991121
3.0	0.294512	0.927086
3.5	0.277663	0.874048
4.0	0.263410	0.829182
4.5	0.251149	0.790584
5.0	0.240454	0.756919
5.5	0.231019	0.727218

Table 3.12: Limits for g_s^τ with $g_p^\tau = \alpha g_s^\tau$ and $\kappa^2 = 2$.

3.3 The $\phi \to \bar{b}b$ decay.

The decay $\phi \to \bar{b}b$ is studied in the same manner as the $\phi \to \tau^+\tau-$ channel, employing the signal strength expression for fermions (equation 2.43). The scalar and pseudoscalar couplings g_s^b and g_p^b are constrained by the experimentally reported signal strength within the range $0.060 \leq \mu_{bb} \leq 0.174$. Applying a 95% Confidence Level, these bounds are scaled by a factor of 1.96, denoted by 1.96σ, resulting in the following limits:

$$0.00528 \leq \mu_{bb} \leq 0.22872 \tag{3.3}$$

The parameter $\kappa_z^2 = \frac{\mathcal{B}^{obs}(Z\to\phi Z)}{\mathcal{B}^{theo}(Z\to\phi Z)}$, which encodes the ratio between observed and theoretical Branching Ratios of the $Z \to \phi Z$ interaction, is retained in the signal strength expression to evaluate the influence of this ratio on the domain of g_s^b and g_p^b. We analyze three scenarios for $\kappa_z^2 = 1, 0.5, 2$, taking the fermion mass $m_f = m_b = 4.18$ GeV.

3.3.1 Case 1: $\kappa_z^2 = 1$

Figure 3.16 plots the permitted values for g_s^b and g_p^b with $\kappa_z^2 = 1$; this is when $\mathcal{B}^{obs}(Z \to \phi Z) = \mathcal{B}^{theo}(Z \to \phi Z)$. The result is a nearly circular ring, with a central exclusion zone that forbids low values of both couplings simultaneously.

The information in table 3.13 complements figure 3.16 by fixing g_p^b and determining the permitted range for g_s^b; this behavior reflects the constraint imposed by the signal strength. Note that the greater the influence of $|g_p^b|$, the smaller the range of g_s^b. Another detail is that in $g_p^b = 0$, the values of $g_{s,min}^b$ and $g_{s,max}^b$ can be switched if their signs become negative. Table 3.14 explores the case where $g_p^b = \alpha g_s^b$, being α a constant of proportionality. It is evident that as α increases, the range for g_s^b reduces accordingly.

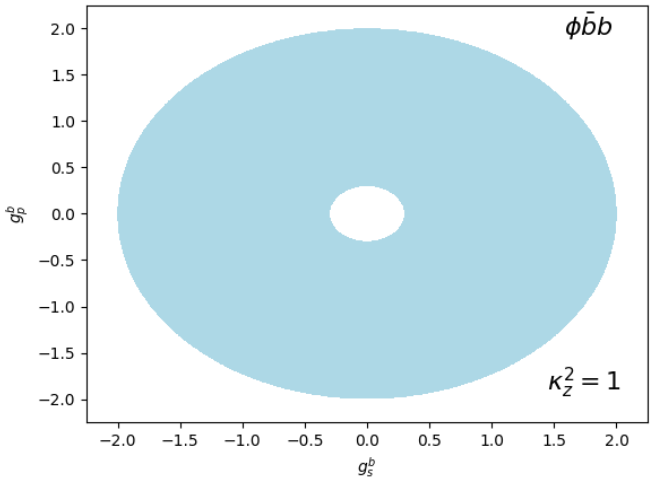

Figure 3.16: Permitted values for g_s^b and g_p^b with $\kappa_z^2 = 1$ in the $\phi \to \bar{b}b$ decay.

g_p^b (GeV)	$g_{s,min}^b$ (GeV)	$g_{s,max}^b$ (GeV)
-1.991381	0	0
-1.593105	-1.199443	1.199443
-1.194829	-1.599257	1.599257
-0.796552	-1.832179	1.832179
-0.398276	-1.958682	1.958682
0	0.303734	1.999072
0.302565	-1.975863	1.975863
0.796552	-1.832179	1.832179
1.146973	-1.634185	1.634185
1.593105	-1.199443	1.199443
1.991381	0	0

Table 3.13: Limits for g_s^b with g_p^b fixed and $\kappa_z^2 = 1$.

α	$g_{s,min}^b$ (GeV)	$g_{s,max}^b$ (GeV)
0.5	0.247678	1.630134
1.0	0.214358	1.410830
1.5	0.191654	1.261399
2.0	0.174910	1.151199
2.5	0.161906	1.065608
3.0	0.151428	0.996648
3.5	0.142753	0.939548
4.0	0.135415	0.891257
4.5	0.129104	0.849721
5.0	0.123601	0.813499
5.5	0.118746	0.781546

Table 3.14: Limits for g_s^b with $g_p^b = \alpha g_s^b$ and $\kappa_z^2 = 1$.

Figure 3.17 illustrates four scenarios with distinct treatments of g_p^b, plotting the expression of μ_{bb} as a function of g_s^b.

- **Scenario 1** depreciates the CP-violating factor ($g_p^b = 0$ GeV). This causes the domain of g_s^b to be cut by the lower boundary of $\mu_{bb} = 0.00528$ leaving $g_s^b \in [-1.999072, -0.303734] \cup [0.303734, 1.999072]$.
- **Scenario 2** takes $g_p^b = 0.302565$ GeV as the minimum value of g_p^b that allows $g_s^b = 0$. The resulting domain of g_s^b is $[-1.975863, 1.975863]$.
- **Scenario 3** considers $g_p^b = 2g_s^b$, therefore the influence of g_p^b depends on the influence of g_s^b. This implies that there is twice as much influence of the CP-violating term as of the CP-conserving term. The domain for g_s^b again becomes disconnected, constrained to $g_s^b \in [-1.151199, -0.174910] \cup [0.174910, 1.151199]$.
- **Scenario 4** Considers an intermediate influence of CP-violation by taking $g_{p,mid}^b = 1.146973$ GeV, the middle value between $g_{p,min}^b = 0.302565$ GeV and $g_{p,max}^b = 1.991381$ GeV. The resulting domain is continuous but narrower than in scenario 2: $g_s^b \in [-1.634185, 1.634185]$.

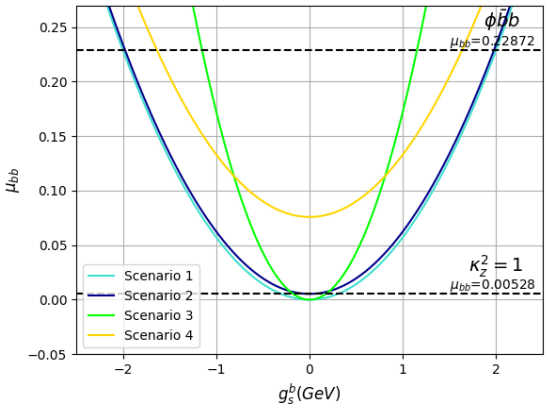

Figure 3.17: Permitted values for g_s^b with g_p^b fixed and $\kappa_z^2 = 1$ in the $\phi \to \bar{b}b$ decay.

3.3.2 Case 2: $\kappa_z^2 = 0.5$

Reducing κ_z^2 to 0.5 relaxes the constraints on the signal strength, thereby expanding the domain of valid couplings g_s^b and g_p^b, as shown in figure 3.18. The general structure of the domain remains a ring-like region with an excluded center.

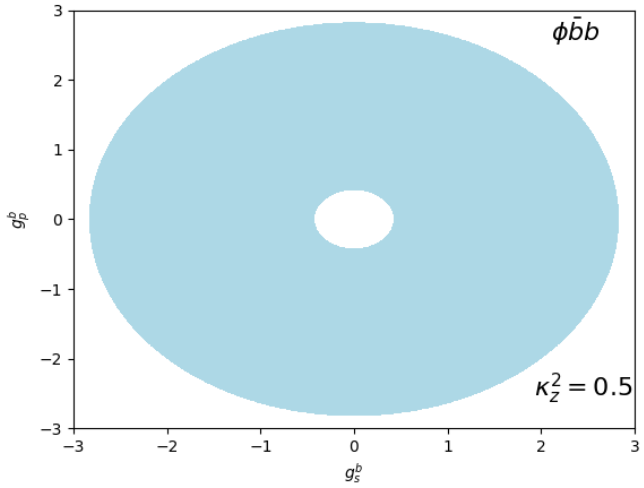

Figure 3.18: Permitted values for g_s^b and g_p^b with $\kappa_z^2 = 0.5$ in the $\phi \to \bar{b}b$ decay.

Tables 3.15 and 3.16 provide numerical constraints for both fixed g_p^b and proportional couplings $g_p^b = \alpha g_s^b$, respectively. The same trends observed in case 1 are reinforced: higher α values lead to narrower g_s^b intervals, and the presence of a central excluded region forces the decoupling of CP-even and CP-odd terms in some regions.

Figure 3.19 displays the four scenarios under the lower κ regime. It confirms the amplification of the permitted regions compared to case 1:

- **Scenario 1** remains disconnected because the CP-odd term is zero, considering that neither g_s^b nor g_p^b can be zero simultaneously, this situation yields to $g_s^b \in [-2.827114, -0.429545] \cup [0.429545, 2.827114]$.
- **Scenario 2** exhibits a wide continuous parabola due to minimal influence of CP-violation $g_p^b = 0.427892$ GeV, which sets a g_s^b domain of $g_s^b \in [-2.794292, 2.794292]$
- **Scenario 3** has the $g_p^b = 2g_s^b$ relation, which yields to a disconnected domain of $g_s^b \in [-1.628041, -0.247360] \cup [0.247360, 1.628041]$.
- **Scenario 4** takes $g_p^b = 1.622065$ GeV as a medium influence of the CP-violating factor, which restricts the domain of g_s^b to $[-2.311086, 2.311086]$.

g_p^b (GeV)	$g_{s,min}^b$ (GeV)	$g_{s,max}^b$ (GeV)
-2.816238	0	0
-2.252991	-1.696269	1.696269
-1.689743	-2.261691	2.261691
-1.126495	-2.591093	2.591093
-0.563248	-2.769995	2.769995
0	0.429545	2.827114
0.427892	-2.794292	2.794292
1.126495	-2.591093	2.591093
1.622065	-2.261691	2.261691
2.252991	-1.696269	1.696269
2.816238	0	0

Table 3.15: Limits for g_s^b with g_p^b fixed and $\kappa_z^2 = 0.5$.

α	$g_{s,min}^b$ (GeV)	$g_{s,max}^b$ (GeV)
0.5	0.350270	2.305358
1.0	0.303148	1.995215
1.5	0.271039	1.783887
2.0	0.247360	1.628041
2.5	0.228969	1.506997
3.0	0.214152	1.409473
3.5	0.201883	1.328722
4.0	0.191506	1.260428
4.5	0.182581	1.201687
5.0	0.174798	1.150461
5.5	0.167932	1.105273

Table 3.16: Limits for g_s^b with $g_p^b = \alpha g_s^b$ and $\kappa_z^2 = 0.5$.

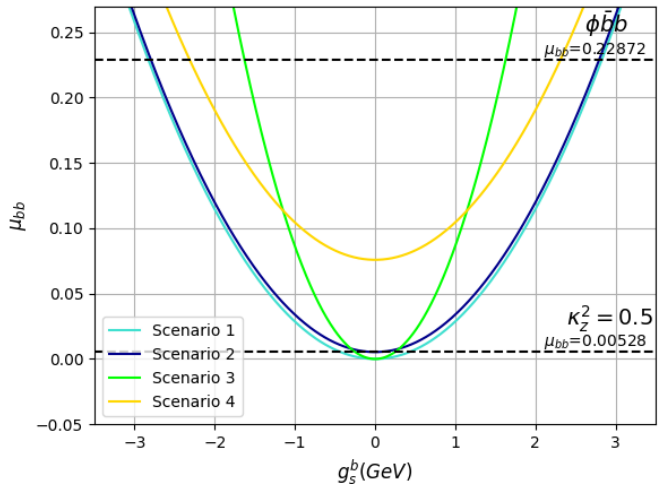

Figure 3.19: Permitted values for g_s^b with g_p^b fixed and $\kappa_z^2 = 0.5$ in the $\phi \to \bar{b}b$ decay.

3.3.3 Case 3: $\kappa_z^2 = 2$

Finally, the case $\kappa_z^2 = 2$ corresponds to $\sigma^{obs}(gg \to \phi) = \frac{1}{2}\sigma^{theo}(gg \to \phi)$, which imposes stronger restrictions on the allowed values of the couplings. Figure 3.20 demonstrates this effect, where the ring-shaped domain significantly contracts and shifts closer to the origin.

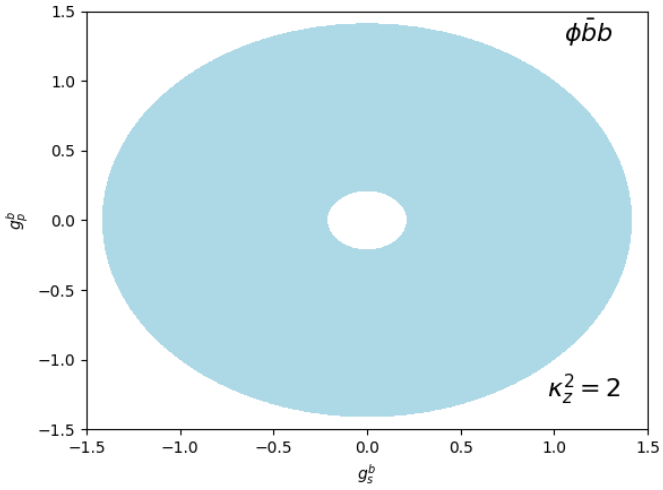

Figure 3.20: Permitted values for g_s^b and g_p^b with $\kappa_z^2 = 2$ in the $\phi \to \bar{b}b$ decay.

Tables 3.17 and 3.18 detail the effects of fixing g_p^b and applying proportional relationships. As expected, the maximum values of g_s^b and g_p^b are reduced considerably compared to the lower-κ cases.

In figure 3.21, the same four scenarios are plotted:

- **Scenario 1** presents a g_s^b domain still disconnected, due to the absence of CP violation. The permitted intervals are $g_s^p \in [-1.413557, -0.214772] \cup [0.214772, 1.413557]$.
- **Scenario 2** allows g_s^b with $g_p^b = 0.213946$ GeV, forming a continuous but narrow domain of $g_s^b \in [-1.397146, 1.397146]$.
- **Scenario 3** Enforces $g_p^b = 2g_s^b$, yielding a symmetric and disconnected domain of $g_s^b \in [-0.814020, -0.123680] \cup [0.123680, 0.814020]$, with stronger a suppression due to the enlarged κ.
- **Scenario 4** Models an intermediate presence of CP violation term ($g_p^b = 0.811033$ GeV), again yielding a continuous but minimal domain: $g_s^b \in [-1.155543, 1.155543]$.

g_p^b (GeV)	$g_{s,min}^b$ (GeV)	$g_{s,max}^b$ (GeV)
-1.408119	0	0
-1.126495	-0.848134	0.848134
-0.844871	-1.130846	1.130846
-0.563248	-1.295546	1.295546
-0.281624	-1.384997	1.384997
0	0.214772	1.413557
0.213946	-1.397146	1.397146
0.563248	-1.295546	1.295546
0.811033	-1.155543	1.155543
1.126495	-0.848134	0.848134
1.408119	0	0

Table 3.17: Limits for g_s^b with g_p^b fixed and $\kappa_z^2 = 2$.

α	$g_{s,min}^b$ (GeV)	$g_{s,max}^b$ (GeV)
0.5	0.175135	1.152679
1.0	0.151574	0.997608
1.5	0.135520	0.891944
2.0	0.123680	0.814020
2.5	0.114485	0.753498
3.0	0.107076	0.704736
3.5	0.100941	0.664361
4.0	0.095753	0.630214
4.5	0.091291	0.600844
5.0	0.087399	0.575230
5.5	0.083966	0.552636

Table 3.18: Limits for g_s^b with $g_p^b = \alpha g_s^b$ and $\kappa_z^2 = 2$.

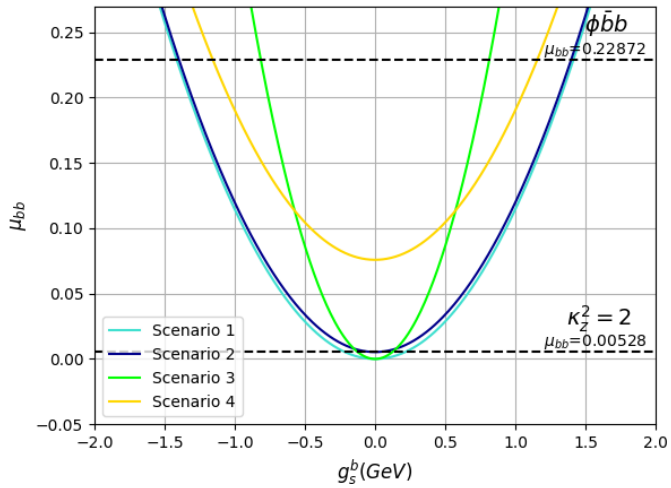

Figure 3.21: Permitted values for g_s^b with g_p^b fixed and $\kappa_z^2 = 2$ in the $\phi \to \bar{b}b$ decay.

Chapter 4

Conclusions

The characterization of the properties of the scalar particle ϕ, possessing a mass of approximately 95.4 GeV, occurs through equations that describe its production and decay channels. This thesis focuses on the decay channels $\phi \to \gamma\gamma$, $\phi \to \tau^+\tau^+$, and $\phi \to \bar{b}b$, where form factors h_i and coupling constants g_s and g_p are explicitly represented within these equations. By determining the permissible values for the parameters associated with these decays, we concurrently apply constraints to the equations themselves. This study is motivated by experimental anomalies observed by CMS, ATLAS, and LEP, with the aim of constraining the effective couplings and properties of the hypothetical particle ϕ and exploring potential deviations from Standard Model predictions.

The analysis of the $\phi \to \gamma\gamma$ decay revealed numerical constraints on CP-conserving ($h_1^{\gamma\gamma}$) and CP-violating ($h_3^{\gamma\gamma}$) form factors, manifesting as circular domains in scenarios 1 and 3, and ring-shaped domains in scenarios 2 and 4. The influence of the production channel, encapsulated in the κ^2 factor, was notably significant in the ranges of permitted values for modules $h_1^{\gamma\gamma}$ and $h_3^{\gamma\gamma}$, which in turn limit the domain areas of $h_1^{\gamma\gamma}$ in the scenarios studied, while their forms are maintained. Similarly, the fermionic decays ($\phi \to \tau^+\tau^-$ and $\phi \to \bar{b}b$) demonstrated precise ranges for scalar and pseudoscalar couplings (g_s,g_p), with their values being strongly dependent on the κ^2 factor. Unlike the form factors h_i, these couplings are real parameters; thus, more precise ranges can be delineated by analyzing the behavior of the scalar coupling (g_s) across the four scenarios previously considered (for the $h_3^{\gamma\gamma}$ factor) concerning the CP-odd factor (g_p). Specifically, in the absence of production channel influences ($\kappa^2 = 1$, $\kappa_z^2 = 1$), the permissible ranges for the modules of $|h_1^{\gamma\gamma}|$ and $|h_1^{\gamma\gamma}|$ in the context of $\phi \to \gamma\gamma$ decay are identified as $|h_1^{\gamma\gamma}| \in [0, 0.129790]$ and $|h_3^{\gamma\gamma}| \in [0, 0.259580]$. In scenarios pertinent to fermions, the allowable values for g_s^τ and g_p^τ are described by $g_s^\tau \in [-2.623561, 2.623561]$ and $g_p^\tau \in [-2.621740, 2.621740]$, whereas for g_s^b and g_p^b are: $g_s^b \in [-1.999072, 1.999072]$ and $g_p^b \in [-1.991381, 1.991381]$.

These results impose rigorous limits on the allowable parameter space of models that expand upon the Standard Model, particularly those involving extra scalar states or CP violation. Scenarios that have been analyzed with significant CP-violating contributions or modified Higgs couplings can now be more accurately targeted or excluded by future collider experimental analyses, guiding efforts in exploring new physics. This study, however, considered simplified assumptions such as fixed κ-ratios and overlooked certain higher-order corrections. Additionally, experimental uncertainties in current datasets limit the definitiveness of some derived constraints, highlighting the need for further refined measurements. Future studies may expand the analysis to include other promising decay modes, such as $\phi \to ZZ^*$ and $\phi \to W^+W^-$. Enhanced statistical analyses incorporating updated datasets from future LHC runs or higher-energy colliders are strongly recommended to further constrain or potentially validate the existence of this scalar particle. Overall, the analysis presented herein provides critical phenomenological constraints and insights into the potential existence of a light scalar boson at 95.4 GeV, significantly advancing our understanding and guiding future investigations for physics beyond the SM.

Bibliography

[1] ALEPH, DELPHI, L3 and OPAL Collaborations. "Search for the Standard Model Higgs Boson at LEP". In: *Physics Letters B* (2003), pp. 1–2. arXiv: hep-ex/0306033 [hep-ex]. URL: http://arxiv.org/abs/hep-ex/0306033.

[2] Adam Alloul et al. "FeynRules 2.0 - A complete toolbox for tree-level phenomenology". In: *Comput. Phys. Commun.* 185 (2014), pp. 2250–2300. DOI: 10.1016/j.cpc.2014.04.012. arXiv: 1310.1921 [hep-ph].

[3] T. Biekötter, M. Chakraborti, and S. Heinemeyer. "A 96 GeV Higgs Boson in the N2HDM". In: *arXiv preprint* (2019). arXiv: 1903.11661 [hep-ph].

[4] Thomas Biekötter, Sven Heinemeyer, and Georg Weiglein. "95.4 GeV diphoton excess at ATLAS and CMS". In: *Physical Review D* 109.3 (2024), p. 035005. DOI: 10.1103/PhysRevD.109.035005.

[5] Thomas Biekötter, Sven Heinemeyer, and Georg Weiglein. "Is there a new Higgs boson at 95 GeV?" In: *arXiv preprint* (2022). arXiv: 2203.13180 [hep-ph]. URL: https://arxiv.org/abs/2203.13180.

[6] Thomas Biekötter, Sven Heinemeyer, and Georg Weiglein. "Mounting evidence for a 95 GeV Higgs boson". In: *J. High Energy Phys.* 08 (2022), p. 201. DOI: 10.1007/JHEP08(2022)201. arXiv: 2203.13180 [hep-ph].

[7] Thomas Biekötter, Sven Heinemeyer, and Georg Weiglein. "The CMS di-photon excess at 95 GeV in view of the LHC Run 2 results". In: *Phys. Lett. B* 846 (2023), p. 138217. DOI: 10.1016/j.physletb.2023.138217. arXiv: 2303.12018 [hep-ph].

[8] Ting-Kuo Chen et al. "A 95 GeV Higgs Boson in the Georgi-Machacek Model". In: *Physical Review D* 109.3 (2024), p. 035005. DOI: 10.1103/PhysRevD.109.035005.

[9] Neil D. Christensen and Claude Duhr. "FeynRules - Feynman rules made easy". In: *Comput. Phys. Commun.* 180 (2009), pp. 1614–1641. DOI: 10.1016/j.cpc.2009.02.018. arXiv: 0806.4194 [hep-ph].

[10] CERN Collaboration. *What's so special about the Higgs boson?* 2025. URL: https://home.cern/science/physics/higgs-boson/what.

[11] CMS Collaboration. *Higgs Boson*. 2025. URL: https://cms.cern/physics/higgs-boson.

[12] CMS Collaboration. "What if there was a second and lighter Higgs boson?" In: *CMS Experiment* (2023). URL: https://cms.cern/news/what-if-there-was-second-and-lighter-higgs-boson.

[13] Georges Aad *et al.* (ATLAS Collaboration). "Observation of a new particle in the search for the SM Higgs boson with the ATLAS detector at the LHC". In: *Phys. Lett. B* 716 (2012), pp. 1–29. DOI: 10.1016/j.physletb.2012.08.020.

[14] Serguei Chatrchyan *et al.* (CMS Collaboration). "Observation of a new boson at a mass of 125 GeV with the CMS experiment at the LHC". In: *Phys. Lett. B* 716 (2012), pp. 30–61. DOI: 10.1016/j.physletb.2012.08.021.

[15] María Teresa Dova. *Que es el bosón de Higgs?* Buenos Aires, Argentina: Editorial Paidós, 2015. ISBN: 978-950-12-9179-1.

[16] John Ellis and Tevong You. "Updated global analysis of Higgs couplings". In: *Journal of High Energy Physics* 2013.6 (2013), p. 103.

[17] David J. Griffiths. *Introduction to Elementary Particles*. 1st ed. Weinheim, Germany: Wiley-VCH Verlag GmbH & Co. KGaA, 2004. ISBN: 978-0-471-60386-3.

[18] Sven Heinemeyer et al. "Light Higgs bosons in the 2HDM with complex Yukawa couplings". In: *Journal of High Energy Physics* 2022.01 (2022), p. 139. DOI: 10.1007/JHEP01(2022)139. arXiv: 2111.04048 [hep-ph].

[19] A. I. Hernández-Juárez, A. Fernández-Téllez, and G. Tavares-Velasco. "New evaluation of the HZZ coupling: Direct bounds on anomalous contributions and CP-violating effects via a new asymmetry". In: *Physical Review D* 107.11 (2023), p. 115031. DOI: 10.1103/PhysRevD.107.115031.

[20] A. I. Hernández-Juárez, R. Gaitán, and R. Martinez. "The H → Z decay and CP violation". In: *arXiv preprint* (2024). arXiv: 2405.03094 [hep-ph]. URL: https://arxiv.org/abs/2405.03094.

[21] W.-Y. Pauchy Hwang. "The Standard Model". In: *arXiv preprint arXiv:1304.4705v3* (2017). Updated August 25, 2017. URL: https://arxiv.org/abs/1304.4705v3.

[22] Instituto de Física de Cantabria (IFCA). *El Bosón de Higgs: 24 preguntas*. https://www.ifca.unican.es. Guía basada en el material del Centro Nacional de Física de Partículas, Astropartículas y Nuclear (CPAN). 2012.

[23] Patrick Janot. "The infamous 95 GeV $b\bar{b}$ excess at LEP: two b or not two b?" In: *Journal of High Energy Physics* 2024.10 (2024), p. 223. DOI: 10.1007/JHEP10(2024)223. arXiv: 2407.10948 [hep-ph].

[24] T. D. Lee. "A Theory of Spontaneous T Violation". In: *Phys. Rev. D* 8 (1973), pp. 1226–1239. DOI: 10.1103/PhysRevD.8.1226.

[25] David Arruga Méndez. *El bosón de Higgs y la ruptura espontánea de simetría*. Trabajo de fin de grado, Universidad de Zaragoza. Departamento de Física Teórica, 2021.

[26] Tania Robens and Tim Stefaniak. "Status of the Higgs singlet extension of the Standard Model after LHC Run 1". In: *Eur. Phys. J. C* 75.3 (2015), p. 104. DOI: 10.1140/epjc/s10052-015-3323-y. arXiv: 1501.02234 [hep-ph].

[27] A Salam. "WEAK AND ELECTROMAGNETIC INTERACTIONS." In: *pp 367-77 of Elementary Particle Theory. Svartholm, Nils (ed.). New York, John Wiley and Sons, Inc., 1968.* (Oct. 1969). URL: https://www.osti.gov/biblio/4767615.

[28] Cecilia Tosciri and ATLAS Collaboration. "$VH(H \to bb)$ Measurements and EFT Interpretation in ATLAS". In: *Journal of High Energy Physics* 2019.5 (May 2019), p. 141. DOI: 10.1007/JHEP05(2019)141. URL: https://link.springer.com/article/10.1007/JHEP05(2019)141.

[29] Unknown. *Higgs Boson Visualization*. Accessed on March 25, 2025. n.d. URL: https://th.bing.com/th/id/OIP.aF_AhAqZdlXpji0_SHwDsAAAAA?rs=1&pid=ImgDetMain.